

Soil Erosion and Reservoir Sedimentation in the Catchment of Wadis in Emirate of Fujairah, UAE – An Integrated Study Using RUSLE, Geospatial Techniques, Sediment and Water Analysis



Subraelu Pakam^{1*}, François Mitterand Tsombou¹, Sachin Ashok Porob¹, Fouad Lamghari Ridouane¹, Simon Zerisenay Ghebremeskel¹, Ahmed Sefelnasr², Kakani Nageswara Rao³, Abdel Azim Ebraheem² and Alaa Ahmed^{2,4}

¹Fujairah Research Center, Sakamkam Road, United Arab Emirates

²National Water and Energy Center, NWECC, United Arab Emirates University, United Arab Emirates

³Department of Geo-Engineering, Andhra University, India

⁴Department of Geosciences, United Arab Emirates University, United Arab Emirates

Submission: March 28, 2025; Published: April 23, 2025

*Corresponding author: Subraelu Pakam, Fujairah Research Center, Sakamkam Road, Fujairah P.O. Box 1626, United Arab Emirates

Abstract

This article discusses the current obstacles associated with dam sedimentation and in overcoming these obstacles to ensure the sustainable management of sediments and water in arid reservoirs for the long term. Consequently, the Revised Universal Soil Loss Equation (RUSLE) model is used to quantify the soil loss in the catchment region in conjunction with terrestrial observations, remote sensing data, and geographic information systems (GIS). The projected annual soil loss in the study area, ranges from 0 to 50 tons per hectare per year ($t\ ha^{-1}\ yr^{-1}$). The findings indicated that 83% of the study area has a low erosion risk, primarily because of the predominance of precipitous terrain and minimal land use. The 14% of the area has a medium erosion risk, while the remaining 3% has a high erosion risk. The wedge method has been used to determine the volume of sediment that was deposited in three major dams: Wadi Hayl Dam, Wadi Ham South Dam, and Wadi Safad Dam. The volume of sediment in Wadi Hayl Dam is $11,570m^3$, the volume in Wadi Ham South Dam is $15,540m^3$, and the volume in Wadi Safad Dam is $12,586m^3$. Sediment and water samples from these reservoirs have undergone examination. In comparison to Wadi Hayl, the Wadi Safad and Wadi Ham sites exhibited significantly higher levels of chemical components in their water samples. The measured variables had a major effect, which are influenced by soil depths, with the 0-25cm range exhibiting more substantial values than the 0-50cm range. Throughout the investigation, the concentrations of heavy metals in the sediment were significantly higher than those in the water samples. The policymakers can utilize the results of this study to implement suitable soil conservation measures in the high and medium-risk soil erosion zones, in addition to the regular maintenance of reservoirs and the utilization of reservoir water and sediment for the benefit of society. The techniques described in this document are therefore applicable to similar environments in arid regions.

Keywords: Field surveys; Water & soil analysis; Soil Erosion model; Remote Sensing & GIS techniques; Wadi flash floods

Introduction

Soil erosion is regarded as one of the most critical environmental issues. Soil erosion is a natural phenomenon that depletes the uppermost layer of soil due to the effects of wind and water erosion [1,2]. Soil erosion diminishes soil fertility, impairs soil conservation methods, and compromises urban infrastructure, hence affecting the sustainability of land and ecosystems [3,4]. The issue is exacerbated by the rising frequency of extreme

rainfall events attributed to recent fluctuations in weather patterns and the escalating impacts of climate change [5,6]. The precise measurement of soil loss in a watershed, essential for effective water and soil management, relies on understanding its influencing elements, including human activities, climatic variability, topography, and soil characteristics [7,8]. In recent decades, it has become evident that soil erosion presents a

substantial threat to long-term soil sustainability, necessitating soil management strategies and effective conservation methods to protect soil from erosive pressures [9-11]. Moreover, anthropogenic soil erosion adversely affects both the environment and the economy [12]. The expansion of agricultural land, linked to population growth, contributes to erosion through deforestation and overgrazing [13]. Erosion can devastate the land, potentially eliminating vegetation that absorbs carbon dioxide, a greenhouse gas that contributes to climate warming [12]. Eroded soil would significantly diminish its carbon concentration, releasing carbon into the atmosphere [14].

It is estimated that 75 billion tons of arable land are lost globally each year [15]. Rainfall is recognized for its extreme spatiotemporal unpredictability and torrentiality in dry regions with limited soil and water supplies. Runoff and sediment load variations are influenced by both human activity and climate variability. It is still very difficult to pinpoint exactly which portion of the observed changes climatic variability and which caused by human activity, though, because the effects of both are integrated at the watershed size [16].

In the Middle East and North Africa (MENA), flash floods are extremely destructive natural disasters even though they are vital sources of groundwater recharge [17]. These MENA countries are deeply concerned about soil erosion and land degradation. Extreme rainfall events induced flash floods as mentioned earlier, cause soil erosion, which is very complex, widespread and dynamic process. Numerous things influence it, including soil type, vegetation, and topography. Construction of water retention/check dams (locally known as breaker dams) is a common procedure in many arid regions, in order to stop these surface flows from emptying into the sea or the desert. Reservoir sedimentation is a major problem at such check dams globally, and it lowers the volume of water that can be stored, putting human and agricultural water supplies at risk. Furthermore, increased water turbidity, clogged hydraulic infrastructure and decreased safety for flood retention are also possible consequences of the soil accumulation at these check dams.

Numerous models, including the Universal Loss Equation (USLE) [19], the revised universal soil loss equation (RUSLE) [20], the Soil and Water Assessment Tool (SWAT) [21,22], the Soil Erosion Model for Mediterranean Regions and the Water Erosion prediction project (WEPP) have been developed and put to use. The widely used empirical model for estimating soil erosion has multiple layers of complexity [18]. RUSLE that is frequently used to forecast soil erosion was created by digitizing and revising the USLE model in the early 1990's [23,24]. Among the three categories of erosion model: conceptual, empirical and physical, USLE and RUSLE are categorized as empirical and conceptual models [25]. Because of its strong dependability, high degree of flexibility, ease of application, accuracy and data accessibility, the RUSLE model has been in use for more than 80 years [26-28]. A number of researchers [29,30] integrated erosion models with the modern

technologies of remote sensing and geographical information systems (GIS) to enhance the precision of erosion estimation and to prepare accurate soil erosion risk maps. Therefore, we used a multiproxy analysis by integrating the remote sensing, GIS and RUSLE model for areas such as Fujairah City, which is taken as a case study, where data on various parameters such as topography, soils, land use are to be generated and modelled to estimate the soil loss.

Keeping view of the above mentioned, satellite remote sensing offers a practical solution. With the ability to explore the same land area on a frequent basis, remote sensing delivers data over large territories. Additionally, by quickly deriving suitable indicators, it can significantly aid in the assessment of regional soil erosion risk [31-33]. Extreme hydrological events cause soil erosion and sediment movement, which is directly related to soil erosion. GIS and remote sensing are widely used in various study areas, primarily in flood risk assessment [34]. [33] (Tzioutzios & Kastridis) states that this work can be accelerated to produce faster, more accurate, efficient, and less time-consuming findings and decisions by utilizing the additional capabilities provided by GIS. Through the application of basic spatial approaches to the datasets and their combination with the RUSLE model, the utilization of GIS and spatial data plays a leading role in this field. GIS and remote sensing make various kinds of spatial data usable. This is supported by recently made accessible remote sensing datasets and GIS technologies, which offer sufficient temporal and spatial accuracy and, in turn, improve flood risk reduction [34]. Furthermore, a few published studies on the use of GIS and remote sensing technologies for soil erosion modeling have been conducted in other regions of the world [35].

As far as the author is aware, no prior work has looked into soil erosion and its deposition in breaker dams, while using the RUSLE model, remote sensing, and GIS analysis in the study region. Also, the dam's sediment and water analysis is not carried out for prior investigations. Therefore, the purpose of this study were: a) To estimate soil erosion in Fujairah City and propose remedies; b) As all three main dams (Wadi Hayl Dam, Wadi Ham Dam, and Wadi Safad Dam) are completely filled with sediment, it is imperative to estimate the amount of sediment (silt) present in the Dams; c) Analyzing the dams sediments and water to determine their physical, chemical, nutrients, and heavy metals present in them. Finally, using the water for irrigation and sediment for agricultural purposes, which will benefit the society.

Study area

The Emirate of Fujairah is the fifth-largest of the seven emirates that make up the United Arab Emirates (UAE). Fujairah, covering over 1450km², is unique in that it is the only emirate having its 90km-long coastline dotted with several rocky headlands jutting into the Gulf of Oman [36,37]. The current research area is a portion of the Fujairah emirate, which has an area of approximately 560km² between 25°17' 31.63" N/25°01'

49.39" N and 56°08' 50.73" E/56°22' 29.12" E (Figure 1a). It is mostly composed of the Fujairah City region, a piece of the Kalba and Khor Fakkan districts of the Sharjah Emirate, and a 77km² area of Oman. The study region exhibits three physiographic zones – a relatively narrow coastal plain and the Hajar/Oman mountain terrain with gently rolling piedmont plain in between. The study area's highest point is 1103m above mean sea level (Figure 1b). Traversed by wadis that originate in the Hajar mountains, they provide substantial amounts of floodwater into the piedmont and coastal plains. Seven wadis, namely, Wadi Hayl, Wadi Saham, Wadi Farfar, Wadi Ham, Wadi Yabsah, Wadi Madhab, and Wadi Safad, run into Fujairah City, along with three main dams, namely Wadi hayl, Wadi ham south dam and Wadi safad dam, apart from several

small breaker dams (Figure 1c) [34]. Of these, Wadi Ham is the longest and the largest wadi in the UAE. It stretches over 30km from Masafi in the northwest to the Wadi Ham Dam in Fujairah City in the southeast and drains an area of 192km² [34]. Wadi Saham, Wadi Farfar, and Wadi Yabsah join Wadi Ham at its dam site (Figure 1c). The Wadi Ham lower plains consist of recent Pleistocene wadi gravels. The consolidated rocks of the Semail formation (Ophiolite sequence) underlie this layer [34]. These wadi beds range from silt to boulders, which are dry for most parts of the year, but when it rains, these become swiftly flowing and roaring rivers carrying huge quantities of sediments washed down from the weathered mountain slopes, thereby getting deposited near the dams.

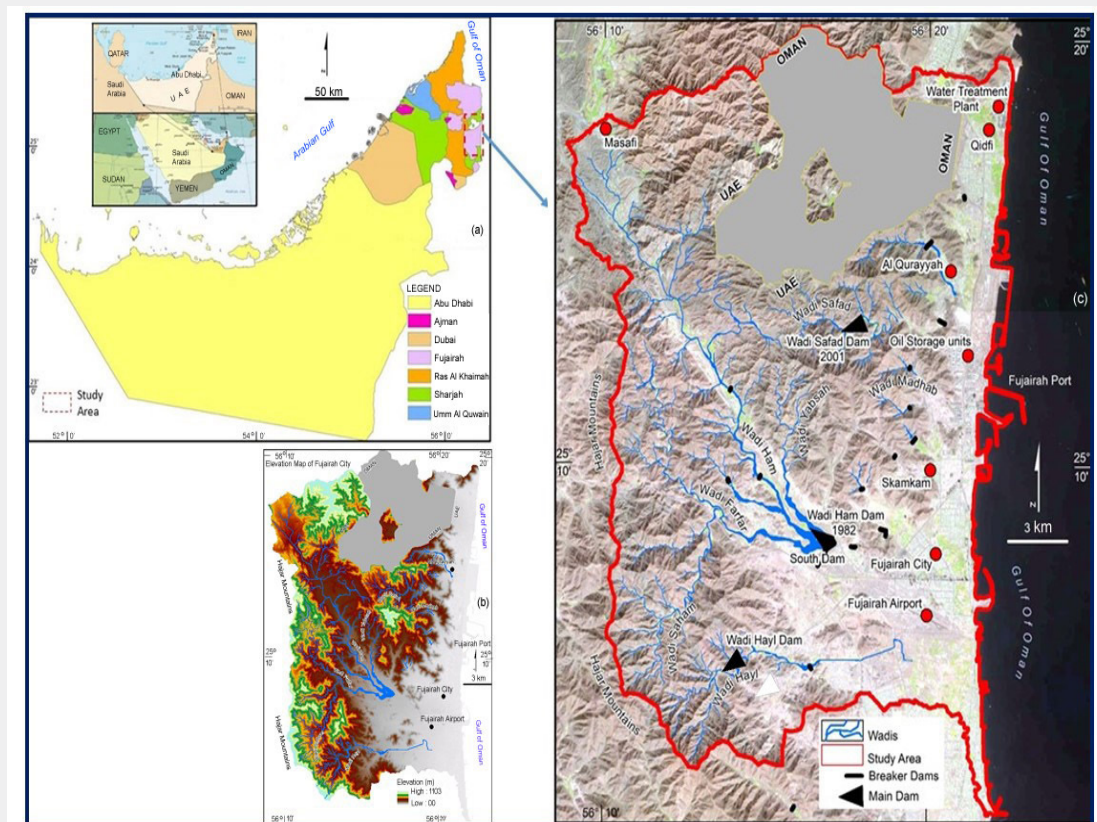


Figure 1: Map of the study area, Inset (a) geographical location of Fujairah City, where study area exists, Inset (b): Elevation of the study area. Inset (c) showing the total catchment areas of seven Wadis, main Dams and Breaker Dams in Fujairah City.

The Fujairah Statistics Center (FSC) for 2023 reports that the population of Fujairah is 318,325; over 77% of this population resides in Fujairah City, the study area [38]. The Fujairah city area is characterized by narrow coastal plains that vary in width from 1 to 3km near central part of the study area and have the widest widths in the northern and southern regions of the research area. Hajar mountains are comprised of Jurassic to Cretaceous igneous and metamorphic rocks in the north and west of the study area, as well as by alluvial deposits at the base of the mountains [39]. The research area has a hyper-arid environment and enjoys a

variety of weather patterns, with summers being hot and muggy and winters being cool to mild. Rainfall in the study area is characterized as erratic and unpredictable and is influenced by orographic effects. The yearly rainfall in the mountainous regions of the west is between 80 and 160mm, which is about 97% of the total yearly rainfall in the northern half of the country [40]. Fujairah often experiences temperatures from 15°C and 47°C in the winter and summer months. A land-sea breeze circulation characterizes the prevailing wind pattern for most of the year, bringing cool sea air to the land. In addition, the average monthly

humidity levels fluctuate between 57% and 78%.

Factors leading to study and map the probable soil erosion areas in the Fujairah City

In arid regions, wadi systems face extreme disasters, including flash floods and droughts, in addition to a lack of comprehensive water and sediment management strategies and monitoring networks. Flash floods are happening more frequently in the northern Emirates, especially in Fujairah City. Convective clouds, local cloud seeding operations, and climate change are all responsible for this. With an average of 160mm in the UAE, the yearly precipitation in Fujairah ranges from 80 to 325mm [41]. Notably, (Figure 2) from CHRS (Center for Hydrometeorology and Remote Sensing) Rainsphere, it shows that the months with the most rainfall in this region are October through April. Figure 3 elucidates yearly average rainfall, and the number on the top of the bar graph indicates the rainy days from (2000-2023), with red

asterisks on top of the bar graph specifying flash flooding events in that year in the Fujairah City region. The graph clearly indicates an increasing trend in the number of rainy days, along with the rise in flooding occurrences, which mostly contributes to soil degradation caused by the rushing waters from the mountains. This increase in the number of rainy days is mostly due to climate change and the UAE’s cloud seeding operations, which significantly began in 2010. It is unavoidable for a hyper-arid nation like the UAE, where rainfall is less than 160mm and high evaporation rates result in a lack of surface water [42]. The Hajar mountains in the eastern part of the UAE were specifically identified as having an apparent rise in rainfall intensities after comparing the pre-cloud seeding era and after [43]. Figure 4 illustrates the number of rainfall days in the region, indicating that the majority of significant high rainfall occurs within a short timeframe, which consequently contributes to soil erosion and the accumulation of sediments in reservoirs.

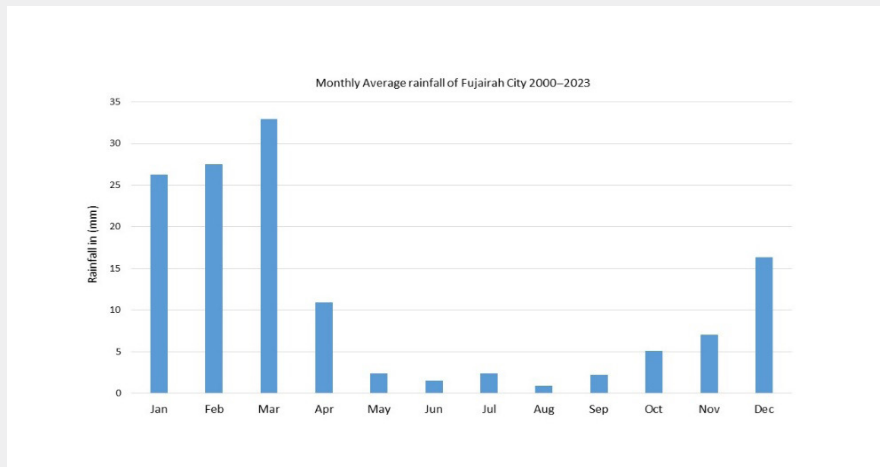


Figure 2: Average monthly rainfall in Fujairah City from 2000-2023.

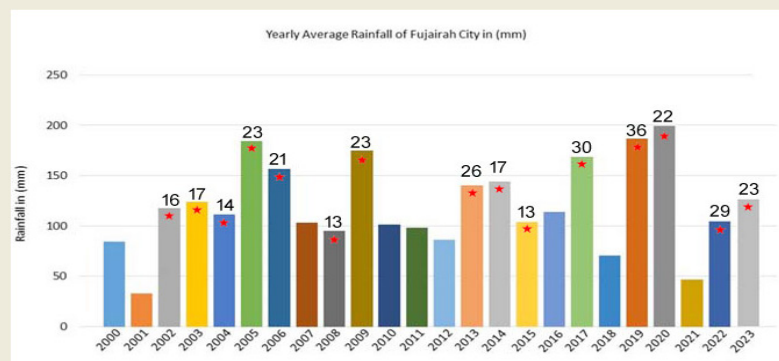


Figure 3: Yearly average rainfall and number of Rainy days in Fujairah City from (2000-2023). Red * and number indicates flooding events and total rainy days in the Fujairah City.

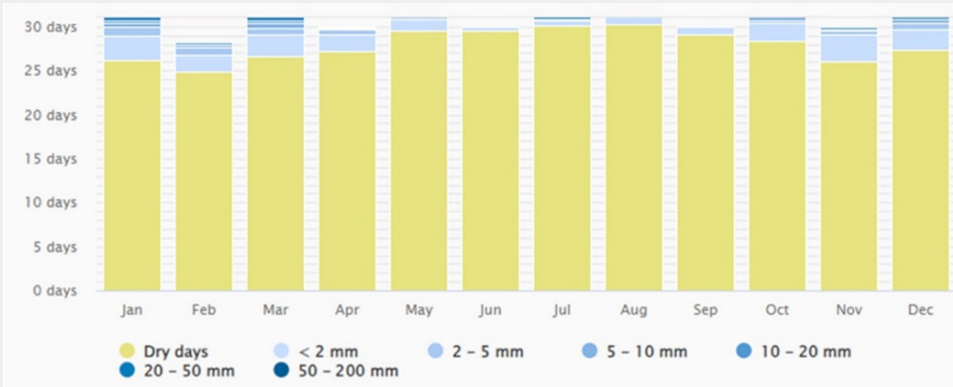


Figure 4: The amount of precipitation is shown in bar graph for Fujairah City (2000-2023) and the number of rainfall days per month.

The most notable flash flood was in July 2022. This flash flood damaged many homes, farms, and infrastructure in the research area. With the aid of 1638 personnel who got impacted by the water, 4225 people in total were evacuated. In addition, more people were given refuge, and 870 more people were rescued. The widespread flooding also affected the third-biggest petroleum bunker center in the world, Fujairah Port [44]. Fujairah has implemented flood control and groundwater recharge structures as part of its mitigating efforts. Nevertheless, the significance of sedimentation in the dams was undervalued, resulting in complications arising from the accumulation of sediment at the top of the dam in the reservoir as shown in (Figure 5), by our on-

site field visits subsequent to the flood incident in July-August 2022 & Mar-May 2024. For instance, at the Wadi Hayl dam, the water level in the reservoir attained 4.5m, resulting in over flowing due to sediment accumulation at the dam. A similar scenario is noted at the Wadi Ham dam as well. Nevertheless, the United Arab Emirates (UAE) is projected to encounter significant levels of sedimentation by the year 2050, which is equal to 1.33% (%/year), which is in the second position in the Middle East; also the highest rate of sedimentation in the Middle East is in IRAN with 1.65% (%/year), and the lowest rate is in Tajikistan having 0.64% (%/year) as indicated by the data from the International Commission on Large Dams [45].



Figure 5: Water spilled over the Fujairah City Dams due to the Sedimentation upto the top of the Dam.

Sedimentation is a significant challenge in reservoir management, particularly in the Fujairah city area, as it is experiencing a rise in intense flash floods. What is the significance of sedimentation in wadi basins in Fujairah? The potential responses are provided below:

- a) The absence of prior research, particularly concerning their effects on reservoirs and infiltration.
- b) The decline in the dam’s capacity to retain water has a direct impact on its ability to serve as a flood prevention measure.
- c) Reducing the infiltration and thereby affecting the replenishment of groundwater.
- d) Enhancing the potential consequences of flash floods in wadis.
- e) In arid environments, particularly in the wadi basins of Fujairah, the aforementioned issues are to be more severe and detrimental compared to perennial rivers due to the influence of climate change.

Hence, it is imperative to evaluate and plot the areas of soil erosion and its detrimental effects of sedimentation in the wadi

basins of Fujairah in order to establish a comprehensive and safe system for managing water and sediment.

Materials and Methods

The methodology combined different approaches from field measurements, geospatial analysis, hydrology and the RUSLE model to assess soil erosion in the catchment areas of seven wadis and to estimate the volume of sediment deposited in the three main dams of Fujairah City, along with analyzing the water and sediments present there. Further, each approach is described in the following sections. For instance, section 4.1, the parameters required for modeling soil erosion, namely rainfall erosivity (R), soil erodibility (K), slope length and steepness (LS), cover management (C), and conservation support practice (P), are introduced to estimate the average annual soil erosion in the catchment area. Table 1 lists the details of the parameters used. After preparing all the parameters, we resample them to a single resolution to facilitate the overlay analysis and ensure accurate results. Additionally, a field investigation on the sediment and water present in the three dams of the Fujairah city area has been analyzed and quantified the volume of the sediment deposited in these dams.

Table 1: Data utilized and description of the data sources.

S. No.	Map Layer	Data Used - Source
1	Rainfall	CHRS (Center for Hydrometeorology and Remote Sensing) RainSphere (http://chrs.web.uci.edu) (2000-2023) (0.25° x 0.25° resolution)
2	DEM	USGS-Earth Explorer website, 30m resolution, (https://earthexplorer.usgs.gov/)
3	Slope	Derived from DEM, 30m resolution
4	Land use / Land cover	Sentinel-2 Satellite Image, 20m spatial resolution, 8 Mar 2023
5	Soil	The World Soil Information - International Soil Reference and Information Centre (ISRIC), resolution of 250m

By calculating the soil erosion parameters, the most often-used erosion model is the RUSLE, which predicts the average yearly soil loss [46]. The RUSLE model, an improved version of the USLE model [47], has been the subject of extensive study and use for many years. Based on the following five parameters, the RUSLE determines the average annual soil loss in tons per hectare per year:

$$A = R \times K \times LS \times C \times P \quad (1)$$

Where A is the average annual soil loss (t/ha/yr), R is the rainfall erosivity parameter (MJ mm/ha/h/year), K is the soil erodibility parameter (ton h /MJ/mm), L is the slope length parameter, S is the slope steepness parameter, C is for the cover and management parameters, and P is for the conservation support practices parameter. Dimensionless parameters are the LS, C, and P (Figure 6). The “Raster Calculator,” a tool found under “Spatial Analyst Tools” in ArcGIS 10.4, was used to prepare the soil erosion map after computing the RUSLE parameters and creating

a raster format for each parameter.

Parameters required for modelling soil erosion

Rainfall erosivity factor (R Factor)

The capacity of rainfall to separate and move soil and small rock particles, so causing soil erosion, is what determines rainfall erosivity (R). R computation requires continuous and comprehensive rainfall data [18]. The length, volume, energy, intensity, and size of raindrops, as well as the pattern of precipitation and the runoff rates that follow, play a big role in the computation of R-factor [48]. The R factor measures the impact of precipitation on the quantity and rate of the runoff factor [33]. The mean yearly rainfall data for the Fujairah city region is used from <https://chrs.web.uci.edu/>. and calculated the rainfall erosivity in the current analysis. CHRS Rainsphere is a comprehensive system that integrates global satellite precipitation data and information. However, we used CHRS data, which covers the whole research

area [34], and an equation from [49] that only required annual precipitation data because there were no precipitation data available for the high terrain regions. This equation produced R-values that were compatible with the equation used in the previously described investigations, i.e., [50,51].

Rainfall erodibility can be computed using the intensity of the rain [52]. However, the lack of high-resolution rainfall data makes calculating the R-factor difficult in most parts of the world [53]. We utilized the equation by Allafta & Christian [54] from the Middle East arid region, which only required annual precipitation data. There were no monthly rainfall data available throughout the study area, especially in the mountainous areas.

$$R = 79 + 0.363 \times X_a \quad (2)$$

The variable X_a represents the mean annual precipitation. The CHRS (accessed on 18 April 2024) data was used to retrieve the annual precipitation of the study region from 2000 to 2023.

Table 2: Soil features and the corresponding K Factor.

S. No	Textural Class	K Factor Values
1	Clay loam	0.6
2	Fine Sand	0.04
3	Sandy clay loam	0.18
4	Loamy Sand	0.4

The inherent ability of soil to withstand erosion from precipitation and runoff is known as soil erodibility, and it is a result of the interactions between the physical and chemical characteristics of the soil that affect detachment, transportation, and infiltration capacity. Among the most significant factors influencing erodibility are the soil's permeability, organic matter content, iron, aluminum, and salt concentrations, as well as its texture and structure [59]. The soil map pertaining to the study area has obtained from The International Soil Reference and Information Center (ISRIC) [60] as a raster image. The study area's soil texture image revealed that loamy sand, clay loam, and sandy clay loam are the most common soil types. Table 2, provided by Stone & Hill Borne [61], has utilized to ascertain their suitable K values. The downloaded image was reclassified in the ArcGIS reclassify tool, using the new K-factor values from Table 2; therefore, the final K-factor raster image is prepared. The distribution of grain sizes in a soil determines its texture.

The K-factor represents a soil's sensitivity to the separation and transfer of soil particles. It illustrates the overall propensity for erosion of a specific soil type and reflects the combined effect of the soil's characteristics [62]. The resistance of soils to erosion varies depending on their qualities. As a result, erodibility varies depending on the physical and biological characteristics of the soil, including its chemical composition, shear strength, aggregate stability, texture, and structure. Based on the current soil types in

The yearly rainfall data were converted to point data, and then the Kriging interpolation method was applied to create the precipitation map. The R factor map was computed based on Equation (2) in ArcGIS 10.4 using the Map Algebra tool in the Spatial Analyst tool, and the R values are cross-verified from other studies in Saudi Arabia [55] and are quite matching.

Soil erodibility factor (K Factor)

Some of the things that make soils in arid regions unique are their poor water-holding capacity, low clay content, high erodibility, high propensity for runoff, hardening, low activity clay, and high summertime surface temperatures [56]. Complex characteristics of arid soils are a reflection of the long-term dynamics and shifting interactions between dissolved ions and water [57]. Mesophytic plant growth and soil formation requires very little water in arid soils [58].

the study area, the corresponding k-factor values for each kind of soil has allocated [63].

Slope length (L) and Slope steepness (S) factor (LS Factor)

The LS factor illustrates how topography impacts erosion and is closely connected to the slope's gradient and length. The Digital Elevation Model (DEM) was utilized in the ArcGIS environment to create the LS factor map [64]. The LS parameter, which is the product of the slope length (L) and slope steepness (slope angle) S, is used to evaluate the impacts of the topography on erosion. As the slope length (L) increases, the overall amount of soil erosion rises due to the increasing runoff buildup on the downslope. Similarly, an increase in the slope steepness was supplemented by an increase in runoff velocity and erosivity [65,66]. The ArcGIS Spatial Analyst plugin calculated the combined LS factor. The SRTM 30m DEM is used to prepare the LS factor raster image, as it is a higher resolution (1 arc-second) of 30m, which is better for local hydrology and terrain analysis. Whereas Aster DEM has a higher vertical error and cannot be used for this analysis. Therefore, the following formula, proposed by the authors of [67,68], was used in the current investigation with an SRTM 30m DEM:

$$LS = (Flow\ Accumulation \times Cell\ Size \div 22.13)^{0.4} \times (\sin\ slope \div 0.896)^{1.3} \quad (3)$$

Where cell size equals the size of the grid cell, sine slope equals the sine of the slope angle in degrees, flow accumulation denotes the cumulative upslope contributing region for a given cell, and LS

equals the merged slope length and slope gradient parameters. We estimated the flow accumulation and slope steepness from the DEM using ArcGIS Spatial Analyst and the Arc Hydro extension. By defining the research region, the DEM data is available at (<https://earthexplorer.usgs.gov/>). After importing the DEM in ArcGIS, UTM projection zone 40 was assigned.

Cover and management (C Factor)

Various soil management techniques can significantly reduce the rate of soil erosion by reducing the velocity of surface runoff, reducing the force of raindrops striking the soil surface, and avoiding the disruptive influence of the rain [69]. Equation (4) was utilized to compute the values of the C factor, which were based on the normalized vegetation cover index values (NDVI) obtained from the Sentinel 2 image [70].

$$C = (1 - NDVI) / 2 \quad (4)$$

Sentinel 2 satellite images of ESA (European Space Agency) provide high temporal resolution and rich multispectral configuration, including 13 spectral bands. It has 4 bands at 10m spatial resolution and six land monitoring bands having a spatial resolution of 20m (blue: 490nm, green: 560nm, red: 665nm, NIR: 842nm, SWIR1: 1910nm, and SWIR2: 2190nm) and three additional bands having 60m spatial resolution covering the red-edge part of the spectrum, which are centered at 705nm, 740nm, and 783nm, and a NIR narrow band at 865nm; therefore, the Sentinel 2 image from March 8, 2023, has been used to extract the NDVI values. The NDVI was derived using the 842nm (NIR) and 665nm (RED) wavelength bands used to show the regional variance in plant cover because it captured both the natural and human-induced conditions of the study area. Equation (5) of NDVI was calculated using the raster calculator tool in ArcTools (ArcGIS 10.4).

$$NDVI = NIR - R / NIR + R \quad (5)$$

Conservation support practice factor (P Factor)

The conservation factor, or P-factor, is the ratio of soil loss in a field employing a certain conservation approach to that of a field not using any conservation strategies. It is a gauge of how well land management techniques are working to lessen soil degradation in a given area [48,71]. Because runoff has the capacity to erode, management practices work to slow down soil erosion by adjusting the conditions, concentration, velocity, and hydraulic forces of it [18]. Therefore, this study considers all plantation and agricultural practices that prevent or lessen soil erosion. The Sentinel 2 image was used for additional processing to create the study area's land use and land cover classes.

Volume estimation of sediment using wedge method in the three main dams in Fujairah City

Watershed management seeks to control the movement of

sediments from various sources to downstream regions [72,73]. The management of watershed drainage systems, particularly breaker dams, influences sediment transport and budgets [74-76]. Breaker dams make it easier for sediment to build up in the upstream along stable wadi beds, which slows the movement of sediment downstream [78]. Shortly after the building of the breaker dam, a sediment wedge begins to accumulate behind the dam, causing the silting upstream to ascend toward the top of the structure. This process typically occurs within a restricted timeframe, frequently less than 30 years [77,78]. Consequently, understanding the sediment wedge volumes retained by breaker dams could effectively aid sediment management at the watershed level.

Measurements of the geometric characteristics of the three main breaker dams (Wadi Hayl, Wadi Ham south dam, and Wadi Safad) and the corresponding wedge model is used for the quantification of the retained sediment volumes *V*. To this purpose, the prism method [79] (Castillo et al. 2007) was used. This method considers the volume of a triangular prism (Figure 8). The volume '*V*' is calculated using the following equation:

$$V = 1/6 * h * L (2A + A') \quad (6)$$

Where *h* and *A* are respectively, the height and the width of the breaker dams, *L* and *A'* are the length and the upstream width of the sediment wedge.

Methodology for the Dams Soil and Water analysis

Water samples were obtained from three dams in the Emirate of Fujairah: Hayl, Safad, and Ham. The collection of samples occurred one time at three distinct locations inside each water body during the dry season (May-June). The obtained water samples were stored in polyethylene bottles and subsequently transported to the Fujairah Research Centre laboratories for chemical analysis. Before collection, we rinsed each usable polyethylene bottle three times with the sampling water to prevent contamination. One liter of water sample was collected in a plastic bottle, carried in a cooler to the laboratory, and thereafter stored at 4°C for future use.

The calibration process for the entire analysis involves preparing standard solutions at specified concentrations of 0.5ppb, 1ppb, 5ppb, 10ppb, 20ppb, and 50ppb for heavy metals and 0.5ppm, 1ppm, 5ppm, 10ppm, 20ppm, and 50ppm for minerals. These calibration standards are used to generate a calibration curve, which establishes the instrument's response at different concentration levels, allowing for precise determination of unknown sample concentrations. To verify the accuracy and reproducibility of the results, duplicate sample testing is performed where the same sample is analyzed twice under identical conditions. The agreement between duplicate results helps assess method precision and detect any potential analytical errors or instrument drift, ensuring data reliability.

Water analysis

Chemical analysis was carried out on the water samples as per the methodology described by Thillai et al. [80]. The collected water samples have been analyzed for pH, electrical conductivity, total dissolved solids, and salinity levels. The Aquasearcher equipment measures these characteristics. According to the study by Voica et al. [81], the water samples were tested for Ca, K, Mg, Ba, Be, Cd, Cr, Pb, Sb, Sn, and Fe. Additionally, the water samples from the three locations were analyzed for total nitrogen levels in accordance with SOP-3090-003.

Soil analysis

All soil sample analysis followed in compliance with the references [82-86]. To conduct the analysis of soil particle sizes, firstly, the sieves were properly cleaned to eliminate any residual particles and contaminants between the several examined samples. Subsequently, 500g of each soil sample were, kept in shaker sieves for 10 minutes. The sieve numbers were 6, 8, 10, 16, 30, 40, 50, 100, and 200, and the pan. We determined the percentage of retained soil on each sieve and used it to estimate the soil particle fractions.

$$\text{Percentage retained soil} = \frac{\text{Weight of retained soil}}{\text{Total soil}} \times 100 \quad (7)$$

Determination of soil organic matter and organic carbon: We set a muffle furnace set at 550°C and placed a 5g dried soil sample in it for 2 hours. Subsequently, then transferred the crucible containing the ignited sample to a desiccator for cooling to room temperature. Finally, calculated the proportion of organic matter (OM) using the following formula:

$$OM = \frac{(W2 - W3) \times 100}{(W2 - W1)} \quad (8)$$

W1 denotes the weight of the crucible; W2 represents the weight of the crucible and sample prior to ignition; and W3 indicates the weight of the crucible and sample subsequent to ignition. We subtracted the percentage of organic carbon from the organic matter composition. Water retention capacity: The soil's water retention capacity got assessed using the droplet counting method. In summary, 50 grams of dried soil sample were placed in a beaker, followed by the addition of 25ml of water, which was thoroughly mixed. Subsequently, the analyzed soil sample was conveyed to the funnel containing filter paper, followed by the careful addition of 25ml of water to the soil. The funnel was affixed to the rubber hose, which had a stopper secured to its neck. Thereafter, the examined sample was permitted to rest in the funnel for 30 minutes, after which the stopper was removed from the rubber hose, allowing it to drain for a further 30 minutes. The collected drop-off water was contained in a measuring tube. The water retention capacity was determined based on the varying volumes. Chemical analyses (pH, electrical conductivity, total dissolved solids, and salinity): The chemical analyses conducted

were executed at a ratio of 1:5 (w/v). Five grams of dried dirt were placed in a 50ml tube, followed by the addition of 25ml of deionized water. Subsequently, the analyzed samples were left to remain undisturbed for 24 hours. Subsequently, soil extract was utilized to ascertain the values of pH, electrical conductivity (EC), total dissolved solids (TDS), and salinity using the Ohaus Aquasearcher equipment. Analyses of minerals and metals (Ca, Mg, Ba, Be, Co, Cr, Ga, Hg, Li, Pb, Sn, and V) were conducted in accordance with SOP, ICP-MS, 2005, and the research work conducted by Aydemir et al. [87].

Data analysis

The gathered data were analyzed in triplet, and a one-way ANOVA was performed to evaluate the impact on the chemical analysis of the sampled water. Two-way ANOVAs were conducted to evaluate the effects of location and soil depth on the physicochemical parameters of the analyzed soil samples. Pearson correlation was also conducted to ascertain the types of correlations among the various examined variables in the soil samples. All data analysis was performed using SYSTAT 13.0.

Limitations and uncertainties

This section addresses several critical limitations of our research methods, including regional applicability, model uncertainty, input data, and validation.

The simple empirical nature of the model and its many subcomponents, data availability concerns, and the model's inability to account for soil loss due to gully erosion, mass sliding events, or the prediction of potential sediment yields in streams are just a few of the limitations and uncertainties in this study that can be linked to the current RUSLE formulation.

The RUSLE model disregards gully erosion. Gully identification and measurement within the watershed will increase the precision of soil loss estimation for upcoming conservation planning and management initiatives. It was also not done to ascertain the most sensitive input characteristics that direct specific and focused actions [71]. To demonstrate a connection between soil loss and unsustainable soil management practices, more investigation is required into the impact of soil loss on plantation productivity and rural/urban lifestyles. Indeed, using the RUSLE model in conjunction with local viewpoints allowed for the validation of the study's primary finding. Soil, land use/cover, rainfall, DEM, and support practice data were used as input factors. After processing the raster layers to show the pertinent input characteristics on the ArcGIS platform, the inputs were multiplied to determine the average annual rate of soil loss and provide intensity maps for the study region.

Using the raster calculator of the map algebra function and related packages, each component layer was multiplied together in a GIS framework, using the RUSLE formula, to estimate the mean

yearly soil loss after data entry operations and layer organization were completed [88].

The water and sediment samples from the three locations Wadi Ham south dam, Wadi Hayl, and Wadi Safad are collected once for the analysis as per the project scope. In the future, more samples to be collected to understand the seasonal changes.

Results

In this study, we estimated the amount and spatial distribution of soil erosion in the study region using remote sensing, GIS methodologies, and the RUSLE model. In addition, five factors related to the risk of erosion were computed.

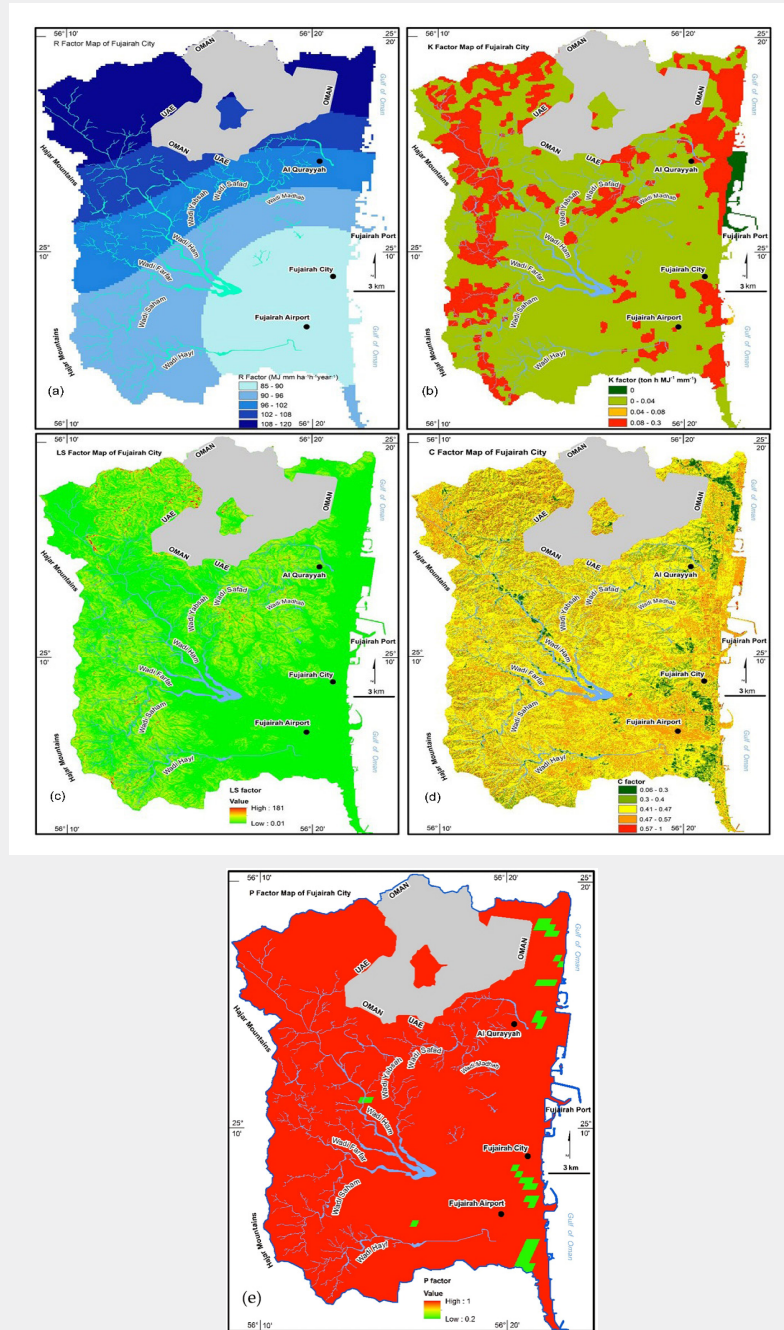


Figure 6: Showing different RUSLE parameters

(a): Spatial distribution of R factor; (b): Spatial distribution of K factor; (c): Spatial distribution of LS factor; (d): Spatial distribution of C factor; (e): Spatial distribution of P factor.

Rainfall erosivity factor (R-Factor)

To calculate the rainfall erosivity (R factor), average rainfall data is utilized. The R factor varied from 85 to 120 MJ mm/ha/h/year. The study area's average annual rainfall pattern has a southerly gradient, and the greatest values are in the northern regions. As a result, a high R factor is expected in the study area's northern regions because R rises there while falling in the southern regions (Figure 6a). However, it did demonstrate that evaluating soil erosion in light of future land use/cover changes and climate change requires consideration of rainfall erosivity. Therefore, the distribution and intensity of inter-annual rainfall, as well as climatic variations, are to blame for this.

Soil erodibility (K factor)

Because clay-rich soils are difficult to separate, their K values are low. Despite their easy disintegration, coarse-grained soils like sand have a low K value because of their potential for runoff. Because they break down more easily and produce more runoff, medium-grained soils like loamy soils have higher K values [89,90]. The K factor for the study area is separated into four groups. The areas that these categories 0.04, 0.04, 0.08, and 0.08-0.3 occupy in the present study area are 413.16, 1.9, and 132.56 km², respectively (Figure 6b). Coming to the western region, where the majority of wadis originate, as well as in its eastern regions, where sandy clay loam is represented, the K factor was elevated, and it's been validated from the field photographs showing considerable erosion in these areas.

Slope length (L) and Slope steepness (S) (LS Factor)

Although it depends more on slope than flow accumulation, the LS factor was computed by taking both flow accumulation and slope into account as inputs (Equation 3). The impact of the topography component on soil erosion is described by the LS factor. It takes soil erosion into account with respect to a certain area's topography. In this case, the topographic aspect represents the study area's vulnerability to topographic erosion. It illustrates how the length and steepness of the slope affect the erosion mechanism (Figure 6c). The percentage slope and Wadi's accumulation were entered into the topographic component estimation process. The study area's western and northwest regions have a steep slope. Additionally, the slope maps show regions with significant potential runoff and, consequently, high rates of erosion; these potentials diminish as the slope decreases from a high to a low degree of slope (Figure 6c). Additionally, the LS factor varied from 0.01 to 181. In the western and north western regions of the research area, higher LS factors were prevalent. The phenomenon suggests that the length and steepness of the slope will enhance the amount of soil loss. The calculation of total soil loss in the study area is significantly impacted by the LS factor, according to a comprehensive review of all soil loss components.

The low-lying eastern alluvial plains have the lowest LS values, which is indicative of the influence of the slope on the LS results.

On the other hand, the study area's steeply sloping, complicated western and northwest regions are having the greatest LS values.

Land cover management factor (C factor)

The cumulative effects of trees, plantations, and other land cover regions on land degradation are measured by the C-factor, which has values ranging from 0.06 to 1, according to Molla et al. [91]. There are no dimensions in the C-factor. As far as possible, the C-factor must be calculated using data on land use and land cover from the present, particularly the vegetation cover, which captures the current state of the study area [92]. Coverage of vegetation is thought to be essential for avoiding water erosion. The Normalized Difference Vegetation Index (NDVI) is used to assess the vegetation cover indices [93,94]. The NDVI established the relationship between soil erosion under specific vegetation and soil erosion on bare land. The eastern edge of the study area is where the lower C-values are located, mostly around the city's plantation areas and the floodplains next to the wadis (Figure 6d). Since these locations are really well protected, there are lower C-factor values and thus less erosion. Increased C factor values are seen in the northwest and southwestern regions, which correspond to Wadi Ham's upstream and downstream sections, respectively. These regions have a higher likelihood of experiencing soil erosion. The C-factor is the most significant element in crop management and maybe the most significant factor in the RUSLE model. ArcGIS 10.4 was used to build the C-factor map.

Conservation support practice factor (P factor)

According to the data collected from the field, especially on the details around the coastal plain, the predominant land use is various plantations and built-up areas. In the downslope areas of the Hajar mountains, there were contouring, artificial lakes, and areas of grass patches along the downstream areas. The purpose of these efforts is to manage the excess rainwater. The LULC thematic layer has been prepared by onscreen digitization, and a slope map is generated using DEM, which is used to calculate the P values, and a P factor raster image was prepared as per Tariq & Qin [95]. Conservation practices (P-factor), is based on the current land management practices used in the Fujairah city region and its environs; the P-factor values varied from 0.2 to 1, as shown in (Figure 6e). Thus, 0.2 represents a very strong facility for protection against erosion, like plantation areas, and other land use areas and 1 represents no facility for protection against soil erosion [96,97]. Based on the results, lower P-factor values characterized the core area of the study area, and higher P-factors characterized the upper and western parts of the study area, comprising hilly terrain.

Estimation of potential soil erosion

To evaluate the amplitude and spatial distribution of soil erosion, GIS, remote sensing, and erosion models were combined for the research region. The primary causes of erosion include

rainfall erosivity, slope steepness and length, soil erodibility, land cover management, and soil conservation. Figures 6a-6e display the modeling results of these factors. Rainfall erosivity modeling shows that an area's propensity for erosion increases with rainfall intensity. The soil erodibility parameter, which shows the soil's susceptibility to erosion as well as the rate of runoff, indicates that the soils with the highest K parameter values are the least transport-resistant and produce the most runoff. The length and gradient of the slope are modeled, and the results show that the larger the runoff velocities and consequent erosion, the steeper the slope. Barren lands have the highest values, while plantations and built-up land use have the lowest, according to the cover and management component [46], which shows how different LULC types affect soil loss rates. The annual erosion map of the study area is displayed in (Figure 7), which is a consequence of the final soil loss model and aids in identifying the regions that are

vulnerable to soil erosion. This study found that the yearly erosion rates in tons per hectare were as follows: high (3% of the area), moderate (14% of the area), and low (83% of the land), covering 483km². Sandy clay loam regions, under development, and sections of barren land are associated with significant rates of soil loss. It is evident that there is a large potential for soil erosion in the downstream portions of the study area, which corresponds to the coastal plain. Most of the images taken in the field are in areas of high soil erosion, which were used to authorize the accuracy of the soil loss map. This also demonstrates that our GIS and RUSLE model output exhibited a significant level of accuracy. The findings of this study could therefore help with decision-making for better soil management and land protection. The appropriate actions should be taken by municipalities and urban development organizations to carefully mitigate this impact.

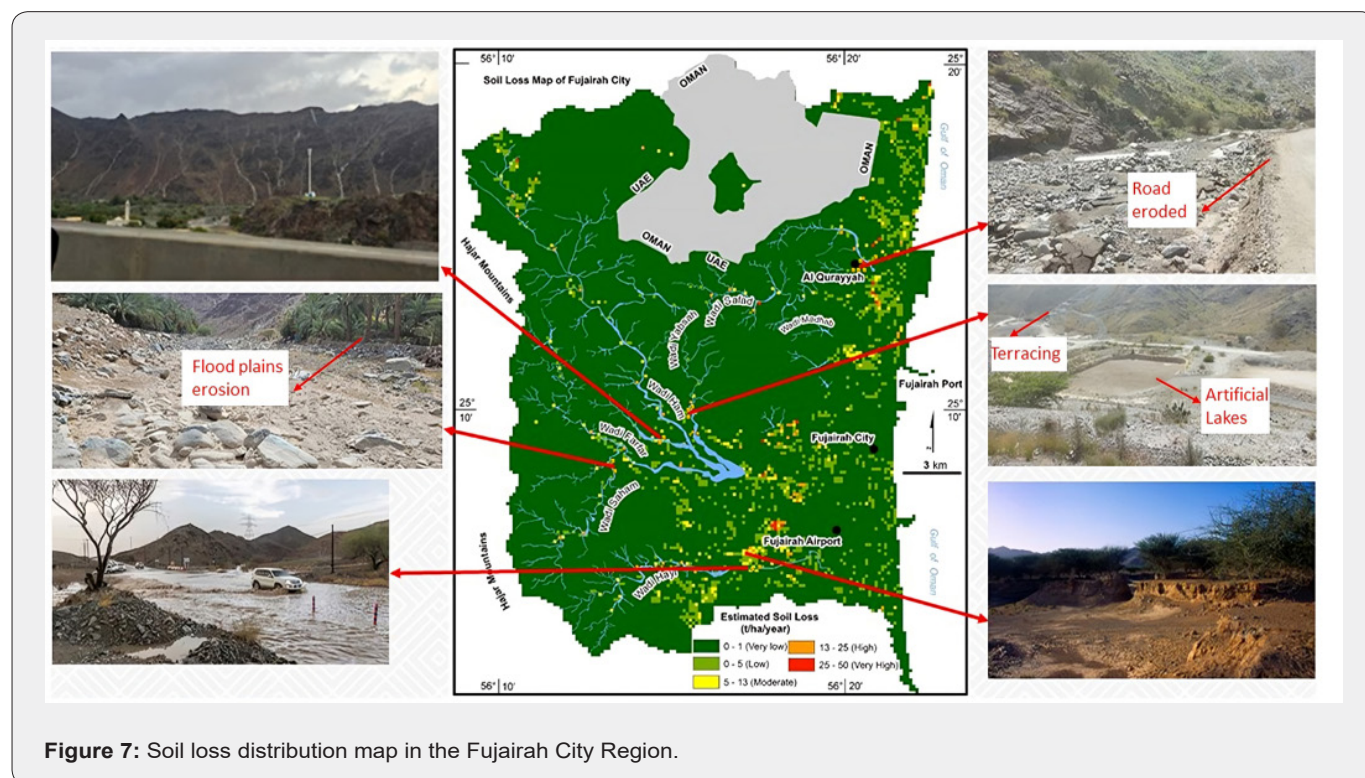


Figure 7: Soil loss distribution map in the Fujairah City Region.

The total annual soil loss estimated in the catchment area is between 25t ha⁻¹ yr⁻¹ to 50t ha⁻¹ yr⁻¹. The soil erosion map is classified into five categories based on erosion risk. The dark green color shows a very low and low potential for soil erosion and is dominantly located in the hilly terrain areas that are mostly towards the west of the study area. The yellow color shows moderate erosion, which is concentrated in the northern and southern parts of the study area. Similarly, the red color shows the high erosion risk areas near the downstream areas of Wadi Ham, Wadi Hayl, and Wadi Safad (25-50 t ha⁻¹ yr⁻¹). According to the results, the basin is experiencing relatively significant spatial

variations in soil loss due to the major differences in topographical conditions, plantation practices, and mainly increased rainfall fluctuations.

Discussion

Discussion on the soil loss in the Fujairah City area

The LS factor map in this work was prepared using an SRTM DEM with a resolution of 30 meters, which was utilized to identify the catchment of seven wadis. The R factor for the study is computed using rainfall data from the CHRS RainSphere during

2000 to 2023. Additionally, the Sentinel-2 data was used to create an LULC classification map and an NDVI map, and the World Soil Information - International Soil Reference and Information Centre (ISRIC) data was used to estimate the K factor.

Both natural and man-made factors contribute to soil erosion [98]. Understanding soil erosion, estimating its magnitude and underlying causes, and devising effective mitigation strategies are essential. Globally, a number of models were created and put forth to measure soil erosion at different spatial scales. For estimating soil losses and sediment transport, RUSLE is a widely recognized, trustworthy technique [99,100]. In arid places where data is scarce, the model efficiently estimates soil erosion with insufficient data [101, 102]. In many local and regional places, erosion is a significant problem, especially in countries with large desert and arid regions, like the United Arab Emirates, which are distinguished by protracted dry seasons [103]. Soil loss is influenced by erosivity, soil erodibility, slope length and direction, and LULC factors—the main parameters used in the RUSLE model to estimate the soil loss [104,105]. Several spatial maps of RUSLE parameters for this study location and utilized to calculate the amount of soil lost.

According to our research, the yearly soil loss in our study region, Fujairah City, is between 25 and 50 t ha⁻¹ yr⁻¹ (Figure 7). Areas of sandy clay loam, areas under development, and barren lands are associated with significant rates of soil erosion. It is also clear that the research areas in the downstream sections, which correspond to the coastal plain, are also in the high soil erosion zones. The foothill areas near the city are also in the moderate erosion zones, where there are already control measures like artificial lakes and terracing already implemented. The results obtained in our study are comparable to many places in the world and in the dry Arabian Gulf region of Saudi Arabia. Recent studies by Elhag et al. [103] on the two dry basins of Yalamlam and Al-Lith in the Kingdom of Saudi Arabia revealed that the annual soil losses in both basins varied from 10t ha⁻¹ yr⁻¹ to 40t ha⁻¹ yr⁻¹. In Wadi El Hayat in the Jizan region, Azaiez et al. [106] monitored soil loss using the FAO and RUSLE models. They discovered that the soil losses ranged from 36.1t ha⁻¹ yr⁻¹ for the FAO equation to 40t ha⁻¹ yr⁻¹ for the RUSLE equation. In order to evaluate soil erosion in the Wadi Yalamlam basin southeast of Jeddah, KSA, Bahrawi et al. [107] employed the RUSLE, RS, and GIS methodologies. They estimated the annual soil loss to be 40t ha⁻¹ yr⁻¹.

The results of our investigation are compared with those from other global investigations. The comparison makes it evident that different regions have different patterns of soil erosion. For instance, the results of this study indicate that the average rate of soil loss in the Fujairah City area is higher than the results of a study by Wolka et al. [108], which found that the average rate of erosion in the Chaleleka Wetland Watershed, Central Rift Valley of Ethiopia, was greater than 50t ha⁻¹ yr⁻¹. However, compared to the average erosion rate of 78t ha⁻¹ yr⁻¹ in Pakistan's Chitral district,

the amount of soil erosion in the Fujairah catchment region is less severe [100]. The Daltonganj Watershed in Jharkhand, India, has an average erosion rate of 69t ha⁻¹ yr⁻¹, according to a different study by Tirkey et al. [109]. In the arid and semi-arid basin of the Oum Er Rbia River (Morocco), Jazouli et al. [110] assessed the average annual soil loss of 58t ha⁻¹ yr⁻¹ in 2023, while the forecasted annual soil loss average for 2030 will be 60t ha⁻¹ yr⁻¹. Significant on and off-site effects of soil erosion include a notable reduction in the land's ability to produce and sedimentation. The quantity of soil erosion, which is mostly influenced by a variety of elements such as vegetation cover, terrain, soil type, and weather, can be blamed for these effects [103,107].

The sediment load and dam management techniques affect the lifespan and performance of the dam. Sedimentation of dams decreases their capacity to hold water, which restricts their usefulness. Thus, accurate sediment load estimation and prompt silt clearance procedures are critical to effective dam management. RUSLE equations have been shown to be effective in a number of models that are presented to assess the sediment load. When making decisions on routine maintenance, rehabilitation, and sediment management strategies, dam operators can utilize this information to evaluate the effects of changing land uses, such as urbanization and deforestation, on soil erosion and sedimentation. By using the suggested models, dam managers can evaluate the sediment loads and improve the sustainability and efficiency of the dam.

Discussion on the sediment wedge calculation in the three main dams in Fujairah city

We have learned that Wadi Ham South Dam, Wadi Hayl Dam, and Wadi Safad Dam experienced water overflowing during the floods of July 2022 and 2024 (Figure 5), due to the sedimentation in these dams. Therefore, in order to gain better understanding of the efficiency of these dams on sediment retention, Diaz et al. [111] presented a methodology based on a topographic survey together with remote sensing and GIS analysis. This method is based on a simple hypothesis since they associate the wedge sediment volume behind these dams with a known geometry. This method strongly relies on the accuracy of data collection, which is only achievable on small scales.

The wedge method employed in this study has proven to be an efficient and reliable approach in determining sediment deposition in these three dams. The discussion below highlights the key findings and implications for future research and sediment management. Measurements of the geometric characteristics of these dams and the corresponding sediment wedge were used for the quantification of the retained sediment behind the dams. These activities necessitate numerous field visits to conduct surveys and determine various variables necessary for volume calculations, in addition to utilizing satellite images and digital elevation models (DEMs). For example, h (height of the dam), and A (width of the

dam) are measured in the field, and L (slope length) is measured from the satellite image, and A' is the slope change length, which

is arrived using the DEM by drawing the vertical profile along the dam and verifying it in the field.

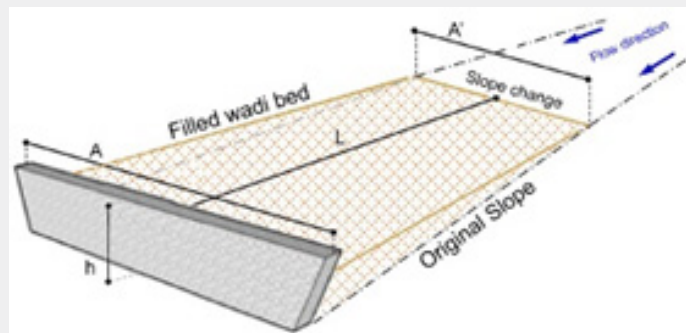


Figure 8: Rough sketch of the sediment wedge volume retained behind the breaker dams.

The measurement values in meters pertaining to individual dams are as follows:

Wadi Hayl dam, h : 4, L : 65, A : 100, and A' : 67.

Wadi Ham south dam, h : 4, L : 63, A : 130, and A' :110.

Wadi Safad dam: h : 4, L : 80, A : 93, A' : 50.

In all of the three dams, wadi Ham south dam has the longest

dam length, whereas Safad dam has the shortest. As per the length of the wedge slope is concerned, Safad has the longest, wadi ham south dam has the shortest. After using the above formula-6 using these values, the volume of sediment deposited in the three dams are calculated. Wadi Hayl dam has a volume of $11,570\text{m}^3$, Wadi Ham south dam has a volume of $15,540\text{m}^3$ and Wadi Safad dam has a sediment volume of $12,586\text{m}^3$.

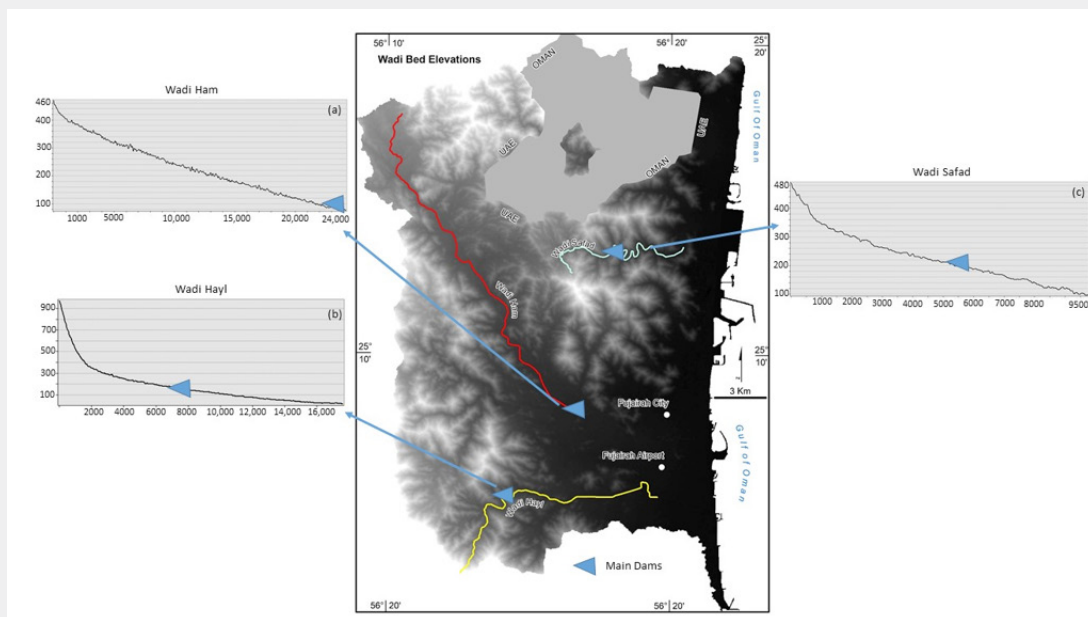


Figure 9: Wadi bed elevations for (a) Wadi Ham, (b) Wadi Hayl, (c) Wadi Safad and the position of the dams analyzed in Fujairah City.

Apart from the calculation of the volume of the sediment behind these dams, the position of these dams in this wadi network is also equally important to understand. Wadi Hayl originated at a height of 950 m above msl, has a total length of 17km before

reaching the coastal plains. Here, the Wadi Hayl dam is constructed at an elevation of 180m and at a distance of approx. 6.8km from its origin point. Whereas, Wadi Ham has started its journey at an elevation of 460m above msl, has a total length of 26km before

reaching the Wadi Ham Dam. Constructed at an elevation of 80m, the Wadi Ham south dam spans 24km from its starting point. Finally, Wadi Safad started its journey at an elevation of 480m above msl, and has a total length of nearly 11km before reaching the coastal plains. Wadi Safad dam is built at a distance of 5.5km from its origin and at an elevation of 212m.

Moreover, after comprehensive field visits, these three wadis have no breaker dams or artificial lakes, before these analyzed dams except wadi Ham. Hence, due to their steep bed slopes (Figure 9abc), the water gushes fast downstream, thereby carrying huge amounts of sediment along with them. Also due to this abrupt power of the water from upstream, there are a lot of erosion areas, like destroyed roads, and culverts, seen in the downstream areas of Wadi Safad and Wadi Hayl.

Discussion on the soil (silt) sedimentation and water analysis in the three main storage Dams in the Fujairah City area

In a world where the climate is changing, managing flood risk, providing enough water, and sediment supply are becoming vital issues. Adequate storage capacity is necessary for reservoirs to be able to manage these hazards [112], and sedimentation gradually reduces this capacity over time [113]. Major influences on surface erosion, land surface stability, and river sediment movement across temporal and geographical scales have been identified as being related to topography, climate, land use, and soils [114]. Sedimentation rates may therefore alter as a result of shifting land use and climate in a reservoir's contributing watershed. This could shorten the reservoir's useful life and make it more difficult

for the reservoir to operate for its permitted uses, such as flood risk management and water supply.

Reservoir sedimentation is a problem, particularly in dry areas where there is a lack of information, monitoring, and efficient management practices. Flash floods are mostly responsible for the formation of erosion and sediment yield in arid environments [115]. However, the effects of flash floods on sedimentation are rarely discussed in these areas, particularly in the Arab countries, which have the highest levels of aridity. Sedimentation causes a number of issues for dam reservoirs and downstream channels, including decreased storage capacity, clogged reservoir beds, and channel damage. Moreover, the conditions around dams in arid locations are different from those in humid regions; in particular, reservoir sedimentation is directly impacted by weathering processes brought on by high temperatures, strong winds, and the erosivity of rainfall and drought. As a result, when infiltration decreases, soil bulk density rises [116]. Because of the sedimentation, dams are unable to hold the floodwater in the reservoir and overflow above the dams in the Fujairah City region (Figure 5). The water is then released to groundwater replenishment downstream of the dam without taking sediment transport into account [117]. Wadi sediments, mainly of Hayl, Ham, and Safad, are rich in nutrients, so it is crucial to understand the nature of the water and silt deposited in the dams in order to use them for domestic and agricultural purposes rather than wasting them for nothing. Therefore, we have taken samples in the three reservoirs and in three different locations (Figure 10) in order to study the water's and soil's physical, chemical, and heavy metal composition.

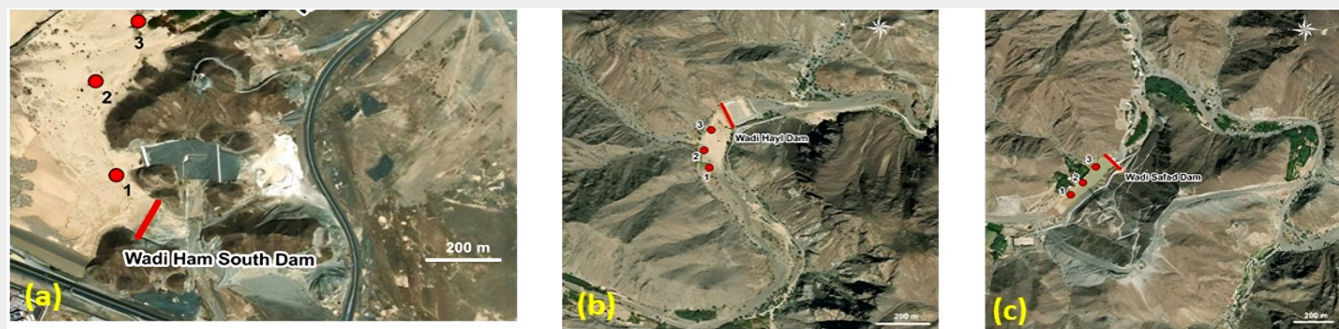


Figure 10: Showing the locations of Soil samples from Wadi Ham-south Dam, Inset (a), Wadi Hayl Dam, inset (b) and Wadi Safad Dam, inset (c).

Water samples analysis

Chemical analysis of the dam's water of Wadi Ham, Wadi Hayl and Wadi Safad

The chemical analysis of the collected water indicated a statistically significant difference ($P < 0.001$) among the various locations (Figure S1 & Table S1). In summary, Hayl dam water exhibited significantly higher values of pH (8.38), electrical conductivity (0.76 mS/cm), total dissolved solids (0.37 g/L), and

sodium (0.00503%) compared to the water samples from Safad and Ham dams. Conversely, nitrogen (0.38 ppm), calcium (18.6%), and potassium (0.15%) concentrations were higher in Ham dam water compared to Safad and Hayl. In contrast to Ham and Hayl, water samples from the Safad dam displayed increased levels of magnesium (5.70%). The water samples from the three locations were analyzed for zinc and copper; however, the tested water exhibited no presence of these chemical components.

Heavy metal analyses of the dam water samples of Hayl, Safad, and Ham in Fujairah after the rain

Locations of dam water samples had substantial effects ($P < 0.05$, $P < 0.001$) on the evaluated heavy metals (Figure S2 & Table S2). Nonetheless, the impacts on beryllium and cadmium elements were not statistically significant ($P < 0.05$). Overall, the water from Ham dam had higher concentrations of Be (0.00669%), Cr (0.0047%), Pb (0.0108%), Sb (0.0018%), and Ti (0.00465%) compared to Safad and Hayl. Observed elevated concentrations of barium (0.00453%) and iron (2.78%) in Safad compared to the water samples from Hayl and Ham dams. Cadmium (0.00017%) concentrations were uniformly distributed among the three examined water sites. The three examined water sample locations were also assessed for Al, As, Co, Mo, Ni, and Sn; nevertheless, the chosen sites exhibited no presence of the analyzed variables.

Soil Samples analysis

To understand how chemical composition varies on each site from water and soil, soil samples are also collected in the same locations for the analyses. The collection was conducted at two different depths that include 0-25cm and 25-50cm. The collection points were distanced by 50m from each other, starting from about 2m from the water body. The collected soil samples are stored in labeled polyethylene bags and sent to the laboratory for further analyses.

Effects of locations (Hayl, Safad, and Ham) and soil depth (0-25 cm, and 25-50 cm) on the chemical analyses of the tested soil samples.

Soil depth and sample collection locations had significant ($P < 0.01$ and $P < 0.001$) effects on the chemical analysis of the tested soil samples (Figure S3 and Table S3). However, no significant ($P < 0.05$) differences were observed on the organic matter and organic carbon when considering the site location. Similarly, no significant ($P < 0.05$) differences were noticeable in the EC, TDS, salinity, organic matter, and organic carbon when emphasizing the soil depths. The interactions between location and soil depths had significant ($P < 0.01$ and $P < 0.001$) effects on pH, TDS, and salinity, magnesium contents, but no significant ($P < 0.05$) differences were recorded on calcium, organic matter, and organic carbon levels. Overall, organic matter (3.605%), organic carbon (2.09%), and pH (8.05) levels were greater in the Safad location between 0-25 cm, and these values were comparably higher than those of 25-50cm and the other locations. Oppositely, water holding capacity (49.33%), calcium (22.5%), and magnesium (4.54%) levels were more important in Ham location between 0-25cm than between 25-50cm, and these readings were higher than those of the other locations. Surprisingly, Ham location exhibited elevated levels of electrical conductivity (325.03 μ S/cm TDS (162mg/L) and salinity (0.15psu) values than in between 0-25cm and the other locations.

Impacts of the locations (Hayl, Safad, and Ham) and soil depth (0-25 cm, and 25-50 cm) on the physical properties of the tested soil in Fujairah

Soil sizes and collection locations had significant ($P < 0.01$

and $P < 0.001$) effects on the physical properties of the tested soil samples regardless of the depth (Figure S4, Table S4). In sum, the three tested locations, Hayl, Safad, and Ham, exhibited higher levels of coarse sand than the other analyzed soil sizes, with Hayl and Ham showing higher values between 25-50cm ($\approx 22\%$). Oppositely, more fine sand (12.12%) and silt and clay (9.58%) amounts were found in Ham location compared with 25-50cm soil depth.

Collection location and soil depths revealed significant ($P < 0.01$ and $P < 0.001$) effects on the water holding capacity (Figure S4(c), Table S5). Nevertheless, the interactions between the two factors had no significant ($P < 0.05$) effects on the assessable variable. Overall, Ham soil sampling showed higher water holding capacity between 0-25cm (49.33%) than 25-50 (47.33%), and these values were greater than the other zones of collections. The lower water holding capacity was noticeable in Hayl location (39.33%).

Heavy metals analysis in the tested soil samples collected in wadi Hayl Dam, Wadi Safad Dam, and Wadi Ham Dam locations.

Soil depths and collection sites significantly influenced ($P < 0.05$, $P < 0.01$, and $P < 0.001$) the heavy metal assessments of the examined soil samples (Figure S5, Table S6). The interactions between soil depths and the collection had substantial impacts ($P < 0.01$ and $P < 0.001$) on the concentrations of barium, cobalt, gallium, lithium, lead, and vanadium, while no significant effects were detected for beryllium, chromium, mercury, and tin. The depth range of 0-25cm demonstrated a greater buildup of the analyzed heavy metals compared to the 25-50cm range, with the Hayl site exhibiting significantly higher concentrations than the other evaluated locations. The concentrations of barium (5.65%), beryllium (0.1%), gallium (3.33%), lithium (1.64%), lead (0.67%), and vanadium (3.16%) were more significant at the Hayl site within the 0-25cm depth compared to the 25-50 cm depth, and these values surpassed those of other sites. The Safad site had elevated tin levels (0.24%) in the 0-25cm depth range compared to the 25-50cm depth and other locations. The concentrations of cobalt (5.81%), chromium (25.5%), and mercury (1.67%) were observed to be elevated at the Ham site inside the 0-25cm depth compared to the 25-50cm depth, and these values surpassed those recorded at other locations. The examined soil samples are evaluated for silver, boron, bismuth, cadmium, and antimony; however, none of these elements was visible in the sampled soils.

Chemical analysis of water and soil samples for the selected locations in Wadi Ham Dam, Wadi Hayl Dam, and Wadi Safad Dam

Sample types and locations had significant ($P < 0.01$ and $P < 0.001$) effects on the tested chemical analyses (Figure S6 and Table S7). However, no significant ($P < 0.05$) effects were recorded on magnesium when considering the sample types variable. Overall, the analyzed water samples exhibited significantly higher levels of chemical elements than the sampling soils. pH (8.38), EC (0.76mS/cm), TDS (0.37g/L), and salinity (0.36psu) were greater

in the Hayl site compared with the other locations and the soil samples. Reversely, magnesium (5.7%) amounts were higher in the Safad location than Ham and Hayl, and the soil, while, calcium (22.5%) levels were more important in the Safad soil compared to the other locations and the water samples.

Overlap heavy metals analyses of water and soil samples collected in Hayl, Safad, and Ham dam

Statistically, sample types and collection locations significantly influenced the evaluated heavy metals ($P < 0.05$ and $P < 0.001$)

(Figure S7, Table S8). The gathered soil samples exceeded the water samples in heavy metal accumulation. Barium (5.67%), beryllium (0.103%), and lead (0.67%) were markedly elevated in the Hayl site in comparison to the other locations and water samples. Conversely, the Ham location demonstrated significantly higher levels of chromium (24.46%) in the soil compared to the other locations and the water samples.

Pearson correlation shows the relationship between the different tested variables in Hayl, Safad, and Ham soil samples (Table 3).

Table 3: Pearson correlation coefficient revealed different types of effects between the tested variables.

	OM	Carb.	WHC	pH	EC	TDS	Sal.	Ca	Mg	Ba	BE	Co	Cr	Ga	Hg	Li	Pb
OM	1																
Carb.	1	1															
WHC	0.379 ns	0.379 ns	1														
pH	0.342 ns	0.342 ns	0.612**	1													
EC	0.348 ns	0.348 ns	0.891***	0.633**	1												
TDS	0.343 ns	0.343 ns	0.890***	0.646**	0.999***	1											
Sal.	0.312 ns	0.312 ns	0.872***	0.606**	0.991***	0.990***	1										
Ca	0.133 ns	0.133 ns	0.546*	0.011 ns	0.250 ns	0.245 ns	0.238 ns	1									
Mg	0.283 ns	0.283 ns	0.801***	0.512*	0.554*	0.555*	0.522*	0.824***	1								
Ba	-0.332 ns	-0.332 ns	-0.717**	-0.644**	-0.898***	-0.901***	-0.882***	0.115 ns	-0.304 ns	1							
Be	-0.338 ns	-0.338 ns	-0.594*	-0.637**	-0.805***	-0.806***	-0.791**	0.254 ns	-0.167 ns	0.949***	1						
Co	0.280 ns	0.280 ns	0.918***	0.397 ns	0.790**	0.788**	0.775**	0.771**	0.878***	-0.536*	-0.372 ns	1					
Cr	0.204 ns	0.204 ns	0.796**	0.130 ns	0.774**	0.763**	0.762**	0.658**	0.658**	-0.518*	-0.369 ns	0.905***	1				
Ga	-0.267 ns	-0.267 ns	-0.691**	-0.412 ns	-0.879***	-0.874***	-0.860***	0.033 ns	-0.286 ns	0.941***	0.875***	-0.577*	-0.678**	1			
Hg	0.112 ns	0.112 ns	0.577*	0.517*	0.323 ns	0.332 ns	0.310 ns	0.725**	0.785**	-0.035 ns	0.010 ns	0.622**	0.338 ns	0.086 ns	1		
Li	-0.368 ns	-0.368 ns	-0.733**	-0.788**	-0.899***	-0.905***	-0.878***	0.104 ns	-0.365 ns	0.975***	0.936***	-0.524*	-0.455 ns	0.871***	-0.155 ns	1	
Pb	-0.201 ns	-0.201 ns	-0.265 ns	-0.471 ns	-0.497 ns	-0.504*	-0.479 ns	0.581*	0.145 ns	0.824***	0.841***	-0.023 ns	-0.012 ns	0.725**	0.359 ns	0.779**	1



Figure 11: Dredging and trucking of the silt from Ham (Inset a) and Safad reservoir (inset b).

Sediment removal options near the breaker dams

There are two main ways to regulate sedimentation in breaker dams: mechanical methods and hydraulic methods. Mechanical methods involve removing sediments from the reservoir. Currently, Wadi Safad and the Main Wadi Ham Dam use mechanical methods like dredging and trucking to remove the sediment (Figure 11). Utilizing the force of flowing water, hydraulic techniques remove silt deposits [118,119]. The act of letting a water flow that contains sediments to pass through a dam in order to remove accumulated sediments is known as flushing [120]. Without requiring costly dredging or other mechanical sediment removal techniques, hydraulic flushing is a very practical method for restoring lost reservoir storage. Two primary categories of flushing exist: First, pressure washing; 2) putting in place drawdown flushing.

a) Pressure Flushing: The process of flushing a system without lowering the water level in the reservoirs is known as pressure flushing. Only a portion of the reservoir is emptied during flushing, even if the water level remains constant. In the lower output zone, where the flushing process is concentrated, a conical shape is formed. This choice is only appropriate for reservoirs with low water-intake capabilities.

b) Drawdown Flushing: With the use of low-level outlets in a dam, drawdown flushing, also known as hydraulic flushing, is a technique for scouring accumulated sediments out of reservoirs either by lowering water levels or not. The bottom gates are used to decrease the reservoir level and raise sediment velocities. There are two types of flushing that fall under this category: free-flow and under pressure. Water is released through the bottom ports during pressure flushing, but the reservoir's water surface level is kept high. Free flow flushing is the process of emptying the reservoir and rerouting the incoming water from upstream through it to replicate the flow characteristics of a natural river.

Conclusion and Recommendation

This study assesses average soil loss on the catchment scale, combining various methodological approaches based on advanced

geospatial technologies, monitoring techniques and empirical models, and also assesses the amount of sediment deposited in the dams, along with dam water and sediment analysis. The RUSLE method has shown potential for predicting soil loss in the seven catchment areas of wadis in Fujairah City using GIS environment and satellite remote sensing data. The total estimated soil loss according to RUSLE was $25\text{-}50\text{t ha}^{-1}\text{ yr}^{-1}$. The spatial variability in rainfall patterns and the corresponding runoff discharges lead to high sediment delivery at the three main dams (Wadi Hayl, Wadi Ham south dam, and Wadi Safad) in Fujairah City. In addition, we have calculated the volume of sediment trapped near the three dams. The trapped sediment volume was estimated to be approximately $11,570\text{m}^3$, $15,540\text{m}^3$ and $12,586\text{m}^3$ in Wadi Hayl dam, Wadi Ham south dam, and Wadi Safad dam, respectively.

Overall, the research's conclusions can help implement appropriate erosion control methods in the areas that are severely affected. The information gathered from this study could assist in creating management scenarios and provide policymakers with options for addressing the risks associated with soil erosion in the Fujairah City area in the most efficient manner. These results lead us to believe that this kind of silt needs to be removed or redirected in order to prevent it from filling the dam reservoir, which will happen very soon, if no maintenance is done with this sediment load, the dam will eventually fail.

Significant differences were found both within and between the examined areas in the water and soil samples that were taken from the Wadi Hayl Dam, Safad Dam, and Ham Dam. The chemical components found in the water samples from the dams at Safad and Ham were much greater than those found in Hayl. The soil analyses revealed the same tendencies. The depth of the soil significantly impacted the measured variables, with 0-25cm revealing higher significant values than 25-50cm. Analyses that overlapped between the soil and water samples revealed the possibility that some chemical components are environment-dependent. Compared to the other elements we studied, heavy metals showed higher in soil deposition than in water

accumulation in our research. The opportunity to investigate the Emirate of Fujairah's environment, with a focus on soil and water samples, was made possible by the current effort, but it would be fascinating to do several further studies that would cover more areas.

In the arid region of the Arabian Peninsula, most of the basins are ungauged; therefore, it is imperative to start the future research projects in the implementation of a statistical model and on field investigations to understand the relation between soil erosion and increase in the rainfall patterns mainly due to climate change, cloud seeding, and assessing the sedimentation. The next stage of the research would be quantifying the amount of sediment deposited for every flash flood event at the major dam areas using open pit, borehole data and drone survey.

Author Contribution

Conceptualization, S.P.; methodology, S.P., F.M.T.; software, S.P., F.M.T.; Validation, S.P., F.M.T., F.L.R., K.N.R.; formal analysis, S.P., S.A.P., A.S.; investigation, S.P., F.M.T., S.A.P., A.S., A.A.E.; resources, S.P., F.M.T., S.Z.G., S.A.P., A.A.; data curation, S.P., F.M.T., F.L.R., A.A.; writing – original draft preparation, S.P., F.M.T.; writing-review and editing, S.P., F.M.T., K.N.R., A.S.; visualization, S.P., A.A.; supervision, S.P., F.L.R., A.A.E.; project administration, S.P., F.M.T., S.Z.G. All authors have read and agreed to the published version of the manuscript

Funding

The Fujairah Research Center, Fujairah has supported this research. The authors would like to thank the journal's editorial board and reviewers for their professional assistance.

References

- Miriam M, Iserloh T, Fister W, Seeger M, Comino JR, et al. (2019). On-Site Water and Wind Erosion Experiments Reveal Relative Impact on Total Soil Erosion. *Geosciences (Switzerland)* 9(11): 1-20.
- Wahla SS, Kazmi JH, Sharifi A, Shirazi SA, Tariq A, et al. (2022) Assessing Spatio-Temporal Mapping and Monitoring of Climatic Variability Using SPEI and RF Machine Learning Models. *Geocarto International* 37(27): 14963-14982.
- Jomaa S, Barry DA, Brovelli A, Sander GC, Parlange JY, et al. (2010) Effect of raindrop splash and transversal width on soil erosion: Laboratory flume experiments and analysis with the Hairsine-Rose model. *J Hydrol* 395(1-2): 117-132.
- Römken MJM, Helming K, Prasad SN (2002) Soil erosion under different rainfall intensities, surface roughness, and soil water regimes. *Catena* 46(2-3): 103-123.
- Borrelli P, Robinson DA, Panagos P, Lugato E, Yang JE, et al. (2020) Land use and climate change impacts on global soil erosion by water (2015-2070). *Proc Natl Acad Sci USA* 117(36): 21994-22001.
- Subraelu P, Sefelnasr A, Yagoub MM, Sherif M, Ebraheem AA, et al. (2022) Global warming climate change and sea level rise: Impact on land use land cover features along UAE coast through remote sensing and GIS. *J Ecosyst Ecography* 12(5): 329.
- Le Bissonnais Y, Cerdan O, Lecomte V, Benkhadra H, Souchère V, et al. (2005) Variability of soil surface characteristics influencing runoff and interrill erosion. *Catena* 62(2-3): 111-124.
- Rudolph A, Helming K, Diestel H (1997) Effect of antecedent soil water content and rainfall regime on micro relief changes. *Soil Technol* 10(1): 69-81.
- Telak LJ, Dugan I, Bogunovic I (2021) Soil management and slope impacts on soil properties, hydrological response, and erosion in hazelnut orchard. *Soil Syst* 5(1): 5.
- Tesfahunegn GB, Ayuk ET, Adiku SGK (2021) Farmers' perception on soil erosion in Ghana: Implication for developing sustainable soil management strategy. *PLoS One* 16(3): e0242444.
- Khalil U, Aslam B (2022) Geospatial-based soil management analysis using novel technique for better soil conservation. *Model. Earth Syst Environ* 8: 259-275.
- Sidi Almouctar MA, Wu Y, Zhao F, Dossou JF (2021) Soil erosion assessment using the rusle model and geospatial techniques (remote sensing and gis) in South-Central Niger (Maradi Region). *Water* 13(24): 3511.
- Emadodin I, Bork H (2012) Degradation of soils as a result of long-term human-induced transformation of the environment in Iran: An overview. *J Land Use Sci* 7(2): 203-219.
- Arabameri A, Pradhan B, Rezaei K, Conoscenti C (2019) Gully Erosion Susceptibility Mapping Using GIS-Based Multi-Criteria Decision Analysis Techniques. *Catena* 180: 282-297.
- Pimentel D, Burgess M (2013) Soil Erosion Threatens Food Production. *Agriculture (Switzerland)* 3(3): 443-463.
- Wang F, Mu X, Hessel R, Zhang W, Ritsema C J, et al. (2013) Runoff and Sediment load of the Yan River, China: Changes over the last 60 yr. *Hydrol Earth Syst Sci* 17(7): 2515-2527.
- Al-Mamari MM, Sameh K, Tahani M, Ali M, Karim A, et al. (2023) Assessment of sediment yield and deposition in a dry reservoir using field observations, RUSLE and remote sensing Wai Assarin Oman. *Journal of Hydrology* 617(Part A): 128982.
- Ganasri BP, Ramesh H (2016) Assessment of Soil Erosion by RUSLE Model Using Remote Sensing and GIS - A Case Study of Nethravathi Basin. *Geosci Front* 7(6): 953-961.
- Renard KG, Foster GR, Weesies GA, McCool DK, Yoder DC (1997) Predicting Soil Erosion by Water: A Guide to Conservation Planning with the Revised Universal Soil Loss Equation (RUSLE); United States Government Printing: Washington, DC, USA.
- Kefi M, Yoshino K, City T (2010) Evaluation of the Economic Effects of Soil Erosion Risk on Agricultural Productivity Using Remote Sensing: Case of Watershed in Tunisia. *Int Arch Photogramm Remote Sens Spat Inf Sci* 38(8): 930-935.
- Lew R, Dobre M, Srivastava A, Brooks ES, Elliot WJ, et al. (2022) WEPPcloud: An Online Watershed-Scale Hydrologic Modeling Tool. Part I Model Description *J Hydrol* 608: 127603.
- de Oliveira Serrão EA, Silva MT, Ferreira TR, Paiva de Ataíde LC, Assis dos Santos C, et al. (2022) Impacts of Land Use and Land Cover Changes on Hydrological Processes and Sediment Yield Determined Using the SWAT Model. *Int J Sediment Res* 37(1): 54-69.
- Panagos P, Ballabio C, Himics M, Scarpa S, Matthews F, et al. (2021) Projections of Soil Loss by Water Erosion in Europe by 2050. *Environ. Sci. Policy* 124: 380-392.
- Kebede YS, Endalamaw NT, Sinshaw BG, Atinkut HB (2021) Modeling Soil Erosion Using RUSLE and GIS at Watershed Level in the Upper Beles Ethiopia. *Environ Chall* 2: 100009.

25. Jha M K, Paudel RC (2010) Erosion Predictions by Empirical Models in a Mountainous Watershed in Nepal. *J Spat Hydrol* 10(1): 89-102.
26. Meliho M, Khattabi A, Mhammdi N (2020) Spatial Assessment of Soil Erosion Risk by Integrating Remote Sensing and GIS Techniques: A Case of Tensift Watershed in Morocco. *Environ Earth Sci* 79: 207.
27. Sandeep P, Kumar KCA, Haritha S (2021) Risk Modelling of Soil Erosion in Semi-Arid Watershed of Tamil Nadu, India Using RUSLE Integrated with GIS and Remote Sensing. *Environ Earth Sci* 80: 511.
28. Dou X, Ma X, Zhao C, Li J, Yan Y, et al. (2022) Risk Assessment of Soil Erosion in Central Asia under Global Warming. *Catena* 212: 106056.
29. Hacısalihoğlu S, Oktan E, Yucesan Z (2010) Predicting Soil Erosion in Oriental Spruce (*Picea Orientalis* (L.) Link.) Stands in Eastern Black Sea Region of Turkey. *Afr J Agric Res* 5(16): 2200-2214.
30. Leh M, Bajwa S, Chaubey I (2013) Impact of Land Use Change on Erosion Risk: An Integrated Remote Sensing, Geographic Information System and Modeling Methodology. *Land Degrad Dev* 24(5): 409-421.
31. Fan J R, Zhang JH, Zhong XH, Liu SZ, Tao HP (2004) Monitoring of Soil Erosion and Assessment for Contribution of Sediments to Rivers in a Typical Watershed of the Upper Yangtze River Basin. *Land Degrad Dev* 15(4): 411-421.
32. Tian YC, Zhou YM, Wu BF, Zhou WF (2009) Risk Assessment of Water Soil Erosion in Upper Basin of Miyun Reservoir, Beijing, China. *Env Geol* 57: 937-942.
33. Tzioutzios C, Kastridis A (2020) Multi-Criteria Evaluation (MCE) Method for the Management of Woodland Plantations in Floodplain Areas. *Int J Geo-Inf* 9(12): 725.
34. Subraelu P, Ebraheem AA, Sherif M, Mirza SB, Ridouane FL, et al. (2023) Risk Assessment and Mapping of Flash Flood Vulnerable Zones in Arid Region, Fujairah City, UAE-Using Remote Sensing and GIS-Based Analysis. *Water* 15(15): 2802.
35. Rawat KS, Mishra AK, Bhattacharyya R (2016) Soil Erosion Risk Assessment and Spatial Mapping Using LANDSAT-7 ETM+, RUSLE, and GIS—A Case Study. *Arab J Geosci* 9: 288.
36. Subraelu P, Ebraheem AA, Sherif M, Sefelnasr A, Yagoub MM, et al. (2022) Land in Water: The Study of Land Reclamation and Artificial Islands Formation in the UAE Coastal Zone: A Remote Sensing and GIS Perspective. *Land* 11(11): 2024.
37. Subraelu P, Yagoub MM, Sefelnasr A, Nageswara K, Allamsatti RS, et al. (2021) Sea-level Rise and Coastal Vulnerability: A preliminary Assessment of UAE Coast through Remote Sensing and GIS. *J Coast Zone Mang* 24(9): 477-480.
38. Yagoub MM, Alsereidi AA, Mohamed EA, Periyasamy P, Alameri R, et al. (2020) Newspapers as a validation proxy for GIS modeling in Fujairah, United Arab Emirates: Identifying flood prone areas. *Nat Hazards* 104: 111-141.
39. Elmahdy SI, Mohamed MM, Ali T (2020) Land Use/Land Cover Changes Impact on Groundwater Level and Quality in the Northern Part of the United Arab Emirates. *Remote Sens* 12(11): 1715.
40. Al-Rashed MF, Sherif MM (2000) Water Resources in the GCC Countries: An Overview. *Water Resour Manag* 14: 59-75.
41. Sherif M, Almulla M, Shetty A, Chowdhury R (2014) Analysis of rainfall, PMP and drought in the United Arab Emirates. *Int J Clim* 34(4): 1318-1328.
42. Mazroui AA, Farrah S (2017) The UAE Seeks Leading Position in Global Rain Enhancement Research. *J Weather Modif* 49: 54-55.
43. Almheiri KB, Rustum R, Wright G, Adeyoye AJ (2021) Study of Impact of Cloud-Seeding on Intensity-Duration-Frequency (IDF) Curves of Sharjah City, the United Arab Emirates. *Water* 13(23): 3363
44. Aliyev E (2022) Fujairah Bunker Ops Remain Disrupted after Flood.
45. ICOLD Sedimentation and Sustainable Use of Reservoirs and River Systems, International Commission on Large Dams (ICOLD), Paris, 2009.
46. Renard KG, Foster GR, Weesies GA, McCool DK, Yoder DC (1997) Predicting soil erosion by water: A guide to conservation planning with the revised universal soil loss equation (RUSLE). In *USDA Agricultural Handbook*; U.S. Department of Agriculture: Washington, DC, USA, No. 703.
47. Wischmeier WH, Smith DD (1978) Predicting rainfall erosion losses. A guide to conservation planning. In *Agriculture Handbook*; US Department of Agriculture: Washington, DC, USA, 537: 85.
48. Farhan Y, Nawaiseh S (2015) Spatial assessment of soil erosion risk using RUSLE and GIS techniques. *Environ Earth Sci* 74: 4649-4669.
49. Choudhury MK, Nayak T (2003) Estimation of soil erosion in Sagar Lake catchment of central India. In *Proceedings of the International Conference on Water and Environment*, Bhopal, India, 15-18; pp. 387-392.
50. Fathizad H, Karimi H, Alibakhshi S M (2014) The estimation of erosion and sediment by using the RUSLE model and RS and GIS techniques (Case study: Arid and semi-arid regions of Dovoraj, Ilam province, Iran). *Int J Agric Crop Sci* 7: 304-314.
51. Mohammadi S, Karimzadeh H, Alizadeh M (2018) Spatial estimation of soil erosion in Iran using RUSLE model. *EcoHydrology* 5(2): 551-569.
52. Amellah O, el Morabiti K (2021) Assessment of soil erosion risk severity using GIS, remote sensing and RUSLE model in Oued Laou Basin (north Morocco). *Soil Sci Annu* 72(3): 142530.
53. Thomas J, Joseph S, Thirivikramji K P (2018) Assessment of soil erosion in a tropical mountain river basin of the southern Western Ghats, India using RUSLE and GIS. *Geosci Front* 9(3): 893-906.
54. Allafta H, Opp C (2022) Soil Erosion Assessment Using the RUSLE Model, Remote Sensing, and GIS in the Shatt Al-Arab Basin (Iraq-Iran). *Appl Sci* 12(15): 7776.
55. Ejaz N, Elhag M, Bahrawi J, Zhang L, Gabriel H F, Rahman K U (2023) Soil Erosion modelling and accumulation using RUSLE and remote sensing techniques: Case study Wadi Baysh, Kingdom of Saudi Arabia. *Sustainability* 15(4): 3218.
56. Rawajfih Z, Khresat SA, Buck B (2005) Arid soils of the Badia region of northeastern Jordan: potential use for sustainable agriculture. *Archives of Agronomy and Soil Science* 51(1): 25-32.
57. Robins C R, Brock-Hon AL & Buck B J (2012) Conceptual mineral genesis models for calcic pendants and petrocalcic horizons, Nevada. *Soil Science Society of America Journal* 76: 1887-1903.
58. Verheye W (2006) Land use, land cover, and soil science - Vol. II, Soils of arid and semi-arid areas.
59. Parysow P, Wang GX, Gertner G, Anderson AB (2003) Spatial uncertainty analysis for mapping soil erodibility based on joint sequential simulation. *Catena* 53(1): 65-78.
60. Moeys J, Shangguan W, Petzold R, Minasny B, Rosca B, Jelinski N, Zelazny W, Souza RMS, Safanelli JL & ten Caten A, Package soil texture In. 2018.
61. Stone RP, Hilborn D (2000) Fact Sheet, Universal Soil Loss Equation; Ministry of Agriculture, Food and Rural Affairs: Guelph, ON, Canada p. 12.

62. Renard K, Foster GR, Wessies GA, Porter JP (1994) RUSLE-Revised universal soil loss equation. *J. Soil Water Conserv* 46(1): 30-33.
63. Rahimi N, Arian M, Ghorashi M (2017) Active Tectonics of the Saymareh-Karkheh River Basin (Northwest of Persian Gulf, Iran). *Open J Mar Sci* 7(2): 238-257.
64. El Jazouli A, Ghafiri A, El Moutaki S, Ettaqy A, Khellouk R (2017) Soil erosion modeled with USLE, GIS, and remote sensing: A case study of Ikkour watershed in Middle Atlas (Morocco). *Geosci Lett* 4: 25.
65. Liu BY, Nearing MA, Shi P J, Jia ZW (2000) Slope length effects on soil loss for steep slopes. *Soil Sci Soc Am J* 64: 1759-1763.
66. Lastoria B, Miserocchi F, Lanciani A, Monacelli G (2008) An estimated erosion map for the Aterno-Pescara river Basin. *Eur Water* 21/22: 29-39.
67. Moore ID, Burch J (1986) Physical basis of the length-slope factor in the universal soil loss equation. *Soil Sci Soc Am J* 50(5): 1294-1298.
68. Moore ID, Burch GJ (1986) Modeling Erosion and Deposition. Topographic Effects. *Trans Am Soc Agric Eng* 29: 1624-1630.
69. Azab YFA, Abbas HH, Jalhoum MEM, Farid IM, Abdelhameed AH, et al. (2021) Soil erosion assessment in arid region: A case study in Wadi Naghamish, Northwest Coast, Egypt. *J Rem Sens Space Sci* 24(3): 1111-1118.
70. Fathizad H, Karimi H, Alibakhshi S M (2014) The estimation of erosion and sediment by using the RUSLE model and RS and GIS techniques (Case study: Arid and semi-arid regions of Doviraj, Ilam province, Iran). *Int J Agric Crop Sci* 7: 304-314.
71. Diwediga B, Le QB, Agodzo SK, Tamene LD, Wala K (2018) Modelling Soil Erosion Response to Sustainable Landscape Management Scenarios in the Mo River Basin (Togo, West Africa). *Sci Total Environ* 625: 1309-1320.
72. Fryirs K (2013) (Dis) Connectivity in catchment sediment cascades: a fresh look at the sediment delivery problem. *Earth Surf Process Landf* 38(1): 30-46.
73. Dumitriu D (2020) Sediment flux during flood events along the Trotuş River channel: hydrogeomorphological approach. *J Soils Sediments* 20: 4083-4102.
74. Diaz-Gutierrez V, Mongil-Manso J, Navarro-Hevia J, Ramos-Diez I (2019) Check dams and sediment control: final results of a case study in the upper Corneja River (Central Spain). *J Soils Sediments* 19: 451-466.
75. Hu J, Zhao G, Mu X, Tian P, Gao P, Sun W (2019) Quantifying the impacts of human activities on runoff and sediment load changes in a Loess Plateau catchment, China. *J Soils Sediments* 19: 3866-3880.
76. Arabkhedri M, Heidary K, Parsamehr M R (2021) Relationship of sediment yield to connectivity index in small watersheds with similar erosion potentials. *J Soils Sediments* 21: 2699-2708.
77. Rosskopf CM, Di Paola G, Atkinson DE, Rodriguez G, Walker IJ (2018) Recent shoreline evolution and beach erosion along the central Adriatic coast of Italy: the case of Molise region. *J Coast Conserv* 22: 879-895.
78. Quinonero-Rubio JM, Nadeu E, Boix-Fayos C, de Vente J (2016) Evaluation of the effectiveness of forest restoration and checkdams to reduce catchment sediment yield. *Land Degrad Dev* 27(4): 1018-1031.
79. Castillo VM, Mosch WM, Garcia CC, Barbera GG, Cano JAN, et al (2007) Effectiveness and geomorphological impacts of check dams for soil erosion control in a semiarid Mediterranean catchment: El Carcavo (Murcia, Spain). *Catena* 70(3): 416-427.
80. Thillai Arasu P, Hema S, Neelakantan MA (2007) Physico-chemical analysis of Tamirabarani river water in South India. *Indian Journal of Science and Technology* 1(2): 1-5.
81. Voica C, Kovacs MH, Dehelean A, Ristoiu D, Iordache A (2012) ICP-MS determinations of heavy metals in surface waters from Transylvania. *Romanian Journal of Physics* 57(7-8): 1184-1193.
82. Kroetsch D, Wang C (2008) Particle size distribution. *Soil Sampling and Methods of Analysis* 2: 713-725.
83. Blazka P, Fischer Z (2014) Moisture, water holding, drying and wetting in forest soils. *Open Journal of Soil Science* 4(5).
84. Bhadha JH, Capasso JM, Khatiwada R, Swanson S, LaBorde C (2017) Raising soil organic matter content to improve water holding capacity.
85. Brischke C, Wegener FL (2019) Impact of water holding capacity and moisture content of soil substrates on the moisture content of wood in terrestrial microcosms. *Forests* 10(6): 485.
86. Sajeeb M I (2021) Soil Texture Analysis and Sediment parameters of Halda River, Chattogram. *Int J Adv Res Biol Sci* 8(8): 19-24.
87. Aydemir D, Simsek G, Ulusu NN (2020) Dataset of the analyzing trace elements and minerals via ICP-MS: Method validation for the mammalian tissue and serum samples. *Data in Brief* 29: 105218.
88. Yesuph AY, Dagneb AB (2019) Soil Erosion Mapping and Severity Analysis Based on RUSLE Model and Local Perception in the Beshillo Catchment of the Blue Nile Basin, Ethiopia. *Environ Syst Res* 8: 17.
89. Prasanna Kumar V, Vijith H, Geetha N, Shiny R (2011) Regional Scale Erosion Assessment of a Sub-tropical Highland Segment in the Western Ghats of Kerala, South India. *Water Resour Manag* 25: 3715-3727.
90. Institute of Water Research, Michigan State University.
91. Molla T, Sisheber B (2017) Estimating Soil Erosion Risk and Evaluating Erosion Control Measures for Soil Conservation Planning at Koga Watershed in the Highlands of Ethiopia. *Solid Earth* 8(1): 13-25.
92. Fagbohun BJ, Anifowose AYB, Odeyemi C, Aladejana OO, Aladeboyeje AI (2016) GIS-Based Estimation of Soil Erosion Rates and Identification of Critical Areas in Anambra Sub-Basin, Nigeria. *Model Earth Syst Environ* 2: 159.
93. Rather M A, Satish Kumar J, Farooq M, Rashid H (2017) Assessing the Influence of Watershed Characteristics on Soil Erosion Susceptibility of Jhelum Basin in Kashmir Himalayas. *Arab J Geosci* 10: 59.
94. Ahmad N, Chaudhry G R (1988) Irrigated Agriculture of Pakistan. In: Nazir S (Ed.), *Shahzad Nazir: Lahore, Pakistan*
95. Tariq A, Qin S (2023) Spatio-Temporal Variation in Surface Water in Punjab, Pakistan from 1985 to 2020 Using Machine-Learning Methods with Time-Series Remote Sensing Data and Driving Factors. *Agricultural Water Management* 280: 108228.
96. Wischmeier WH, Smith DD (1978) *Predicting Rainfall Erosion Losses: A Guide to Conservation Planning*; Department of Agriculture, Science and Education Administration: Corvallis, OR, USA.
97. Ekwueme OU, Obiora DN, Okeke FN, Ibutot C (2021) Environmental Assessment of Gully Erosion in Parts of Enugu North, Southeastern Nigeria. *Indian J Sci Technol* 14(29): 2400-2409.
98. Tsegaye L, Bharti R (2021) Soil erosion and sediment yield assessment using RUSLE and GIS-based approach in Anjeb watershed, Northwest Ethiopia. *SN Appl Sci* 3: 1-19.
99. Maqsoom A, Aslam B, Hassan U, Kazmi Z, Sodangi M, et al. (2020) Geospatial assessment of soil erosion intensity and sediment yield using the revised universal soil loss equation (RUSLE) model. *ISPRS Int J Geo-Inf* 9(6): 356.

100. Saleem U, Amjad A, Muhammad I, Muhammad J, Muhammad I (2018) Geospatial assessment of soil erosion intensity and sediment yield: a case study of Potohar Region, Pakistan. *Environmental Earth Sciences* 77: 1-13.
101. Obaid H, Shahid S (2017) Soil erosion susceptibility of Johor River basin. *Water Environ J* 31(3): 367-374.
102. Tadesse L, Suryabhadgavan K, Sridhar G, Legesse G (2017) Land use and land cover changes and Soil erosion in Yezat Watershed, North Western Ethiopia. *Int Soil Water Conserv Res* 5(2): 85-94.
103. Elhag M, Hidayatulloh A, Bahrawi J, Chaabani A, Budiman J (2022) Using inconsistencies of wadi morphometric parameters to understand patterns of soil erosion. *Arab J Geosci* 15: 1-14.
104. Moses A (2017) GIS-RUSLE interphase modelling of soil erosion hazard and estimation of sediment yield for river Nzoia basin in Kenya. *J Remote Sens GIS* 6(3): 1-13
105. Xu L, Xu X, Meng X (2013) Risk assessment of soil erosion in different rainfall scenarios by RUSLE model coupled with Information Diffusion Model: A case study of Bohai Rim, China. *Catena* 100: 74-82.
106. Azaiez N, Baazaoui N, Blel I, Hammami B (2021) Contribution of the adjusted empirical analysis of the RSULE and FAO models in the estimation of soil losses in the watershed of Wadi El Hayat (Saudi Arabia). *Arab J Geosci* 14: 1-18.
107. Bahrawi JA, Elhag M, Aldhebiani A, Galal H, Hegazy A, et al. (2016) Soil erosion estimation using remote sensing techniques in Wadi Yalamlam Basin, Saudi Arabia. *Adv Mater Sci Eng*.
108. Wolka K, Tadesse H, Garedew E, Yimer F (2015) Soil erosion risk assessment in the Chaleleka wetland watershed, Central Rift Valley of Ethiopia. *Environ Syst Res* 4: 1-12.
109. Tirkey A S, Pandey A, Nathawat M (2013) Use of satellite data, GIS and RUSLE for estimation of average annual soil loss in Daltonganj watershed of Jharkhand (India). *J Remote Sens Technol* 1: 20-30.
110. El Jazouli A, Barakat A, Khellouk R, Rais J, El Baghdadi M (2019) Remote sensing and GIS techniques for prediction of land use land cover change effects on soil erosion in the high basin of the Oum Er Rbia River (Morocco). *Remote Sens Appl Soc Environ* 13: 361-374.
111. Diaz V, Mongil J, Navarro J (2014) Topographical surveying for improved assessment of sediment retention in check dams applied to a Mediterranean badlands restoration site (Central Spain). *J Soils Sediments* 14: 2045-2056.
112. Podolak CJP, Doyle MW (2015) Reservoir sedimentation and storage capacity in the United States: Management needs for the 21st century. *Journal of Hydraulic Engineering* 141(4): 02515001.
113. Kondolf GM, Gao Y, Annandale GW, Morris GL, Jiang E, et al (2014) Sustainable sediment management in reservoirs and regulated rivers: Experiences from five continents. *Earth's Future* 2(5): 256-280.
114. Allen P A (2017) *Sediment Routing Systems*. New York, NY: Cambridge University Press,
115. Walling D, Kleo A (1979) Sediment yields of rivers in areas of low precipitation: A global view. *Proceedings. The Hydrology of areas of low precipitation*.
116. SS Al-Ismaily AK, Al-Maktoumi AR, Kacimov SM, Al-Sagri HA, Al-Busaidi MH, et al. (2013) Morphed block-crack preferential sedimentation in a reservoir bed: a smart design and evolution in nature *Hydrol Sci J* 58(8): 1779-1788.
117. SA Prathapar, AA Bawain (2014) Impact of sedimentation on groundwater recharge at Sahalanowt Dam, Salalah, Oman. *Water Int* 39(3): 381-393.
118. Fan J, Morris GL (1992a) Reservoir sedimentation II: Reservoir desiltation and long-term storage capacity. *Journal of Hydraulic Engineering* 118(3): 370-384.
119. Fan J, Morris GL (1992b) Reservoir sedimentation I: Delta and density current deposits. *Journal of Hydraulic Engineering* 118(3): 354-369.
120. Atkinson E (1996) The feasibility of flushing sediment from reservoirs (Report OD 137, TDR Project R5839), Wallingford.



This work is licensed under Creative Commons Attribution 4.0 License

DOI: [10.19080/IJESNR.2025.35.556408](https://doi.org/10.19080/IJESNR.2025.35.556408)

Your next submission with Juniper Publishers will reach you the below assets

- Quality Editorial service
- Swift Peer Review
- Reprints availability
- E-prints Service
- Manuscript Podcast for convenient understanding
- Global attainment for your research
- Manuscript accessibility in different formats
(Pdf, E-pub, Full Text, Audio)
- Unceasing customer service

Track the below URL for one-step submission
<https://juniperpublishers.com/online-submission.php>